COMPUTATIONAL MODELLING OF MANIFOLD TYPE FLOWSPREADERS

By

Lu Hua

B.Sc., Zhejiang University, P.R.China

A THESIS SUBMITTED IN PARTIAL FULFILLMENT OF

THE REQUIREMENTS FOR THE DEGREE OF

MASTER OF APPLIED SCIENCE

in

THE FACULTY OF GRADUATE STUDIES

DEPARTMENT OF MECHANICAL ENGINEERING

We accept this thesis as conforming

to the required standard

THE UNIVERSITY OF BRITISH COLUMBIA

OCTOBER, 1998

In presenting this thesis in partial fulfilment of the requirements for an advanced degree at the University of British Columbia, I agree that the Library shall make it freely available for reference and study. I further agree that permission for extensive copying of this thesis for scholarly purposes may be granted by the head of my department or by his or her representatives. It is understood that copying or publication of this thesis for financial gain shall not be allowed without my written permission.

Department of Mechanical Engineering
The University of British Columbia
2324 Main Mall
Vancouver, Canada
V6T 1Z4

Date:

Oct. 21, 1998

Abstract

A computational model is developed for the prediction of flow distribution in manifold type flowspreaders. To address the difficulties associated with complex configurations of manifold type flowspreaders and convergence problems, several numerical techniques are used, including curvilinear coordinate-based calculations and domain segmentation. A 3D curvilinear coordinate-based CFD code, called CMGFD, which can be used to calculate laminar/turbulent flows in arbitrary geometries using curvilinear grids is adapted. To support the application of the CMGFD code, a multigrid elliptic grid generation code, MBEGG, was modified to generate multi-block curvilinear grids for the CMGFD code.

Validation of these methods is performed. The calculation of flow in liquid cooling module manifolds shows that the predicted flow rate in each channel is in good agreement with other numerical studies; the calculated cross-stream motions at different locations agree well with experimental data for the turbulent flow modelling in a pipe junction, .

A Canfor manifold type flow spreader, which includes a tapered rectangular duct with 560 tubes, is modelled. The effects of spreader recirculation rate and inlet flow rate on the flow distribution have been considered. The computational results show that the numerical tool has the ability to model the flow distribution of manifold type flowspreaders.

Table of Contents

List of Figures

Nomenclature

C_μ, C_1, C_2	The $k-\epsilon$ turbulence model constants
F^i	Volume flow rates across cell faces (m^3/s)
G	Generation rate of turbulent kinetic energy (kg/ms^3)
$\mathbf{J}$	Generalized flow flux
$P_{i,i=1,2,3}$	Control functions in grid generation equations
$\mathbf{S^i}$	Surface area vectors
U^i	Contravariant velocities
U^{ξ_i}	Tangential velocity components (m/s)
u_τ	Friction velocity, $u_\tau = \frac{\tau_w}{\varrho}$
V	Volume of a control cell (m^3)
$\mathbf{a_i}$	Covariant vectors
$\mathbf{a^i}$	Contravariant vectors
a_{ij}	Coefficients of the grid generation equations
a_{nb}	Coefficients of the discretized governing equations
$\mathbf{e_i}$	Tangential vectors
$\mathbf{e^i}$	Normalized surface vectors
d	Injection orifice diameter (m)
g^{ij}	Surface area metric tensor
k	Turbulent kinetic energy (m^2/s^2)
p	Mean static pressure (kg/ms^2)
$\mathbf{u}$	Velocity vector
x_i	Cartesian coordinates

x, y, z	Cartesian coordinates
y^+	Dimensionless distance from the solid wall, $y^+ = \frac{\varrho y u_\tau}{\mu}$
α_i	Non-orthogonal angles
ϵ	Dissipation rate of turbulent kinetic energy (m^2/s^3)
κ	Von Karman constant, $\kappa = 0.41$
μ	Dynamic viscosity (kg/ms)
ξ_i	Curvilinear coordinates
ϱ	Fluid Density (kg/m^3)
σ_k, σ_ϵ	Turbulence model constants
τ_w	Wall shear stress (kg/ms^2)
ϕ	General dependent variable
Γ	General diffusivity coefficient

Subscript

∞	Main stream
e, w, ...	Center of control volume surfaces
E, W, ...	Control volume center

Superscript

c	Coarser grid
f	Finer grid
ξ_i	ξ_i oriented variables

Acknowledgment

I wish to express a deep sense of gratitude to my supervisors Dr. M. Salcudean and I. S. Gartshore for their encouragement, guidance and support throughout the course of this research. Working with them has been an enjoyable experience which I will cherish throughout my life.

I would like to thank Dr. Suezone Chow, Ed Dylke and Harvey Daryl in Canadian Forest Products Ltd.

I would also like to thank all my colleagues of the CFD group in the Department of Mechanical Engineering, especially Pinfan He and Eric Bibeau. Their suggestions and discussions have been invaluable.

Chapter 1

Introduction

1.1 Background

The headbox is a critical component in the paper-making system. Its purpose is to supply well dispersed stock containing a constant percentage of fibers to all areas of the sheet-forming section. How well this is accomplished depends on the design of the flow approach system and the headbox.

Early designs of headboxes accepted feed flows from either a single or multiple entry points, combined them where necessary, spread them across the width of the machine, and directed the flow towards the slice. Such designs frequently fell short of providing adequate flow uniformity, particularly as machine speeds increased and the demands of cross-machine paper uniformity became more stringent.

Superior results have been achieved in modern headboxes by employing a manifold flowspreader feeding into an array of relatively small diameter tubes. The arrangement is illustrated in Figure 1.1.

The advantages of this system are that it is simple in design, compact, relatively easy to construct and flexible in operation.

A large number of experimental and computational studies have been devoted to the understanding of the manifold flow process in order to achieve more uniform outflow. A brief literature review is provided in Section 1.2 and 1.3.

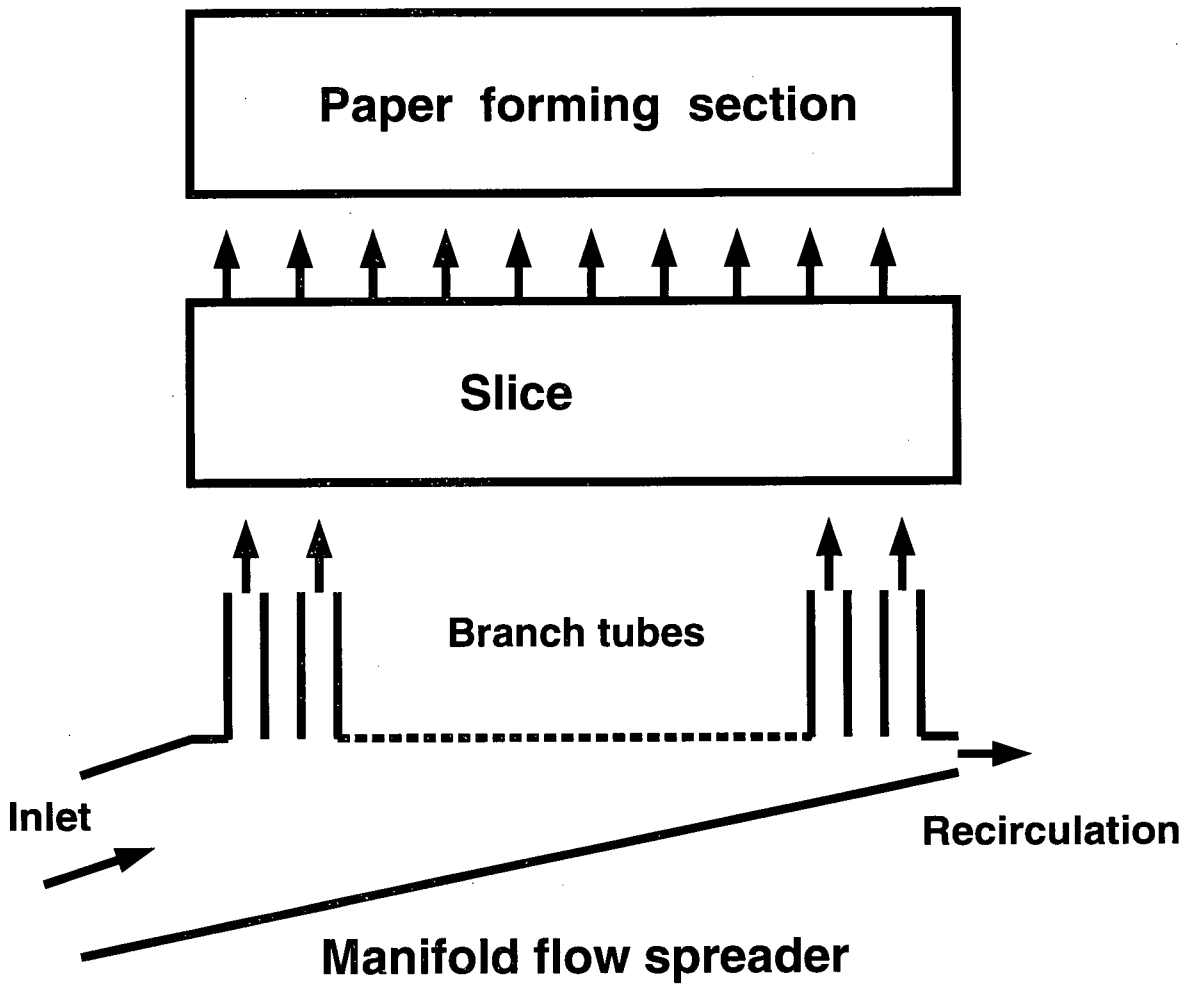

Figure 1.1: Illustration of a manifold flow spreader

1.2 Motivation for the Present Studies

The problem of generating uniform distribution of fluid across a section has preoccupied engineers for a long time. The earliest paper on this subject is that of Enger *et al* (1929).

The concept of the multi-tube manifold type flowspreader was introduced by Mardon and his colleagues during the mid 1950's. The subsequent efforts of Mardon (1963,1971) to popularize and advance this concept have played a large role in the universal adoption of this design.

Manifolds are of two types. The first type includes branching pipes of successively decreasing diameter so that the flow from one large pipe or duct is divided into many smaller ones. The second type involves a tapered header with lateral openings. For this manifold, the difficulty in obtaining uniform distribution is due to pressure build-up at the manifold exit. To prevent the pressure build-up, a portion of the inlet flow is recirculated from the manifold exit. The different manifolds discussed above are illustrated in Figure 1.2.

For the tapered manifold flow spreader, the designer has considerable flexibility in selection of the cross-sectional shape of the manifold, its taper, the design of the tubes and the recirculation rate.

The flow uniformity at the tube exit is influenced by a number of factors. Therefore, in order to achieve an optimal design of the manifold flow system, a parametric analysis has to be performed to determine the manifold performance with various parameters. Experimental measurements are expensive, time-consuming, and limited by the availability and accuracy of the measuring instruments. An alternative method is numerical prediction.

Recent advances in high speed digital computers and computational fluid dynamics make it possible to model the 3-D flow field in manifold flow spreaders.

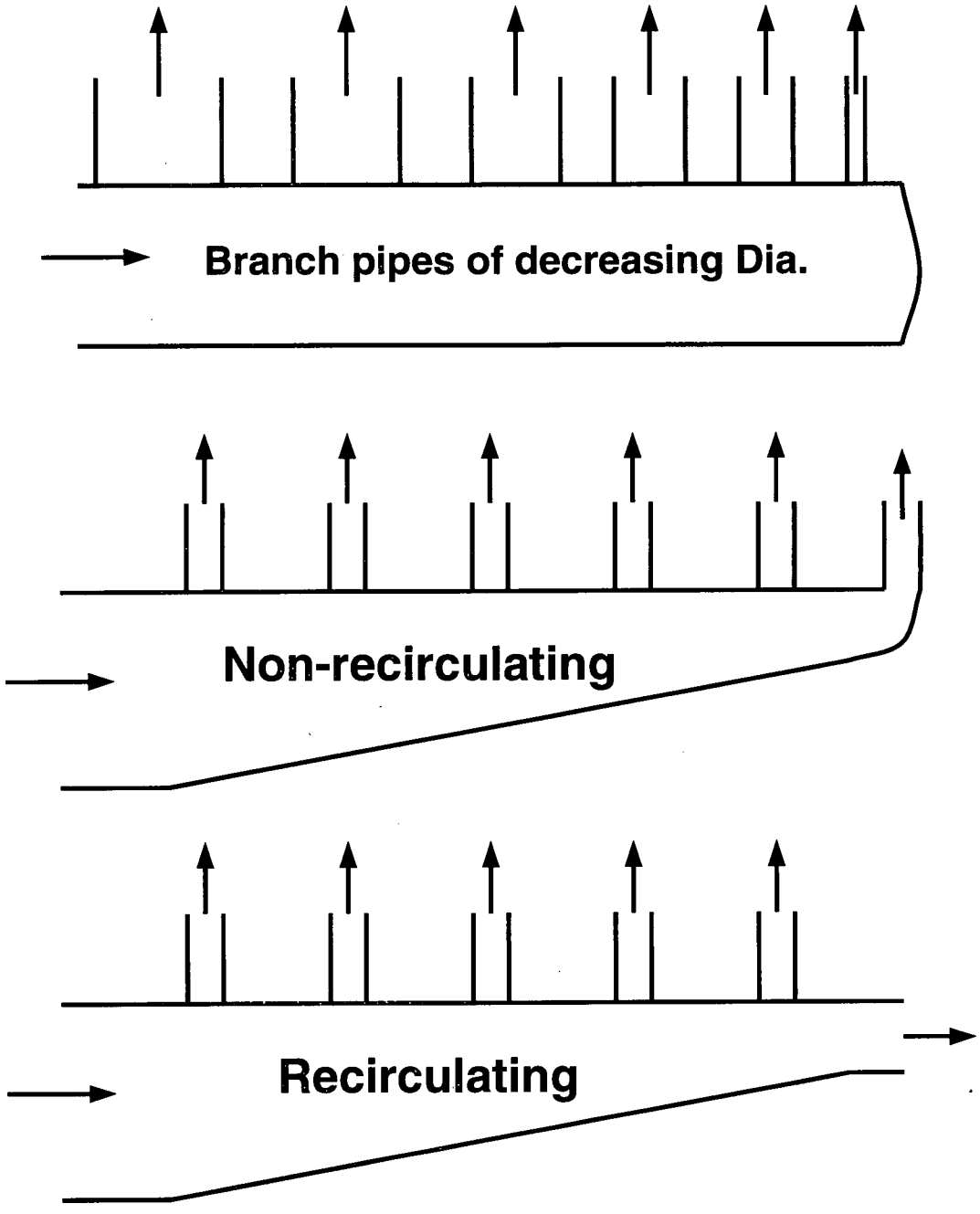

Figure 1.2: Illustration of three different types of manifold

1.3 Previous Numerical Studies

There are a number of manifold numerical studies in the literature. However, most of the early numerical studies are confined to simple 1-D and 2-D geometries.

Among the three-dimensional studies, Syrjala *et al* (1988) used the Phoenics CFD code to model the flow behaviour of a tapered manifold flow spreader (see Figure 1.3 (a)). Their results indicate that the geometry of the header affects the lateral distribution of the discharge mainly near the inlet. They used a slot to replace all branch tubes, so the flow information inside those branch tubes is unavailable. Shimizu *et al* (1992) performed a numerical study on the influence of headbox on paper quality by using the SCKYU CFD code (see Figure 1.3 (b)). They found the adjustment of the recirculation flow rate corrects the flow distribution only on the side near the flow exit, but they also used a slot instead of a row of branch tubes.

Jones *et al* (1988) used FLUENT to predict turbulent flow profile in a straight-channel diffuser as shown in Figure 1.4 (a). Fair agreement with experimental results is reported. Fu *et al* (1992) conducted a numerical study of the flows in a pipe junction (see Figure 1.4 (b)). Three-dimensional turbulent flows through a single branched manifold were simulated using the $k - \epsilon$ model of turbulence. The effects of the flow split ratio and inlet flow rate were investigated.

1.4 Remarks on Manifold flow Studies

Numerical simulations can furnish detailed information about fluid flow and heat transfer phenomena and provide a fast and ecnomical tool for understanding the manifold flow process. However, numerical simulation has not reached a stage where it can be directly applied to manifold design. One of the major problems is that there is a lack of appropriate methods to model the flow spreading process for the complex manifold geometry.

Therefore, the majority of the previous calculations are limited to simplified geometries.

The complex configuration of an actual manifold presents a number of difficulties for numerical simulation. First, the flow region includes a tapered pipe or duct and a number of branch tubes for which an ordinary coordinate system, such as Cartesians or cylindrical coordinate cannot be applied. Secondly, the flow occurs in different flow regions: a main flow region through a tapered pipe or duct and a number of sub-regions in the small branch tubes for which ordinary one-segment methods are ineffective. Thirdly, the diameter of the branch tubes are small compared with the characteristic dimension of the main flow region. When a fairly dense grid is used in the branch tubes, the overall number of grid nodes needed will be too large to be handled by the present computer capacities. The use of non-uniform and dense grid near branch tubes can cause additional convergence difficulties. Therefore, a solution method must be developed to address both the convergence and geometrical difficulties.

The use of a simplified geometry, such as a slot, can provide useful flow information about the complex manifold flow distribution. However, the flow inside the branch tubes is not accounted for in such a model, consequently the manifold flow might be significantly misrepresented.

1.5 Objective and Scope

The objective of the present work is to address the need discussed above to develop an efficient numerical tool suitable for modelling the manifold flow in realistic physical geometry. Numerical simulations can provide detailed information about flow fields and constitute a fast and economical tool for understanding the manifold flow process. The present study is motivated by the above need and is devoted to the numerical simulation of flow in a manifold. It is our aim to develop a computational capability for the prediction

of flow in a manifold having a realistic geometry.

This objective involves development of code and computational methods. Substantial code development work has been done in the CFD group supervised by Dr. Martha Salcudean and Dr. Ian Gartshore, Department of Mechanical Engineering at UBC. The MGFD code, developed by Nowak (1992), is a comprehensive 3D numerical code using multigrid and domain segmentation techniques. However, its application is limited to rectangular type geometry because it is based on the cartesians coordinate system. A 3D curvilinear coordinate based CFD code, which can be used to calculate laminar or turbulent flows in arbitrary geometry using curvilinear grids has been developed by He (1995). In addition, an elliptic grid generation program called MBEGG was developed to generate appropriate grid (see appendix A).

In the present study, several numerical techniques are implemented in the code to simulate the manifold flow spreader. These techniques are described below (see also appendix B for a description of the basic equations).

First, the multigrid elliptic grid generation program is generalized to create grids for the tapered manifold spreader with different cross sectional configurations, as illustrated in Figure 1.5, especially for the manifolds with a circular cross-section (see appendix C). This was a major effort in the present thesis.

Second, several two- and three-dimensional laminar and turbulent flows are computed and compared with other numerical, experimental and analytical results. The objective of this step is to validate that the dividing and combining manifold can be predicted with sufficient accuracy by using the present computational method.

The third step is aimed at the modelling of the manifold tube bank. The Canfor manifold flow spreader model in this study has 7 rows and 80 columns of branch tubes. Instead of simulating all these tubes, a pressure correction method is proposed so that the replacement of the tube tank with ten large similar tubes can give fairly reasonable

results. The performance of the method is investigated through several computational examples. The main work in this step is presented in Chapter 3.

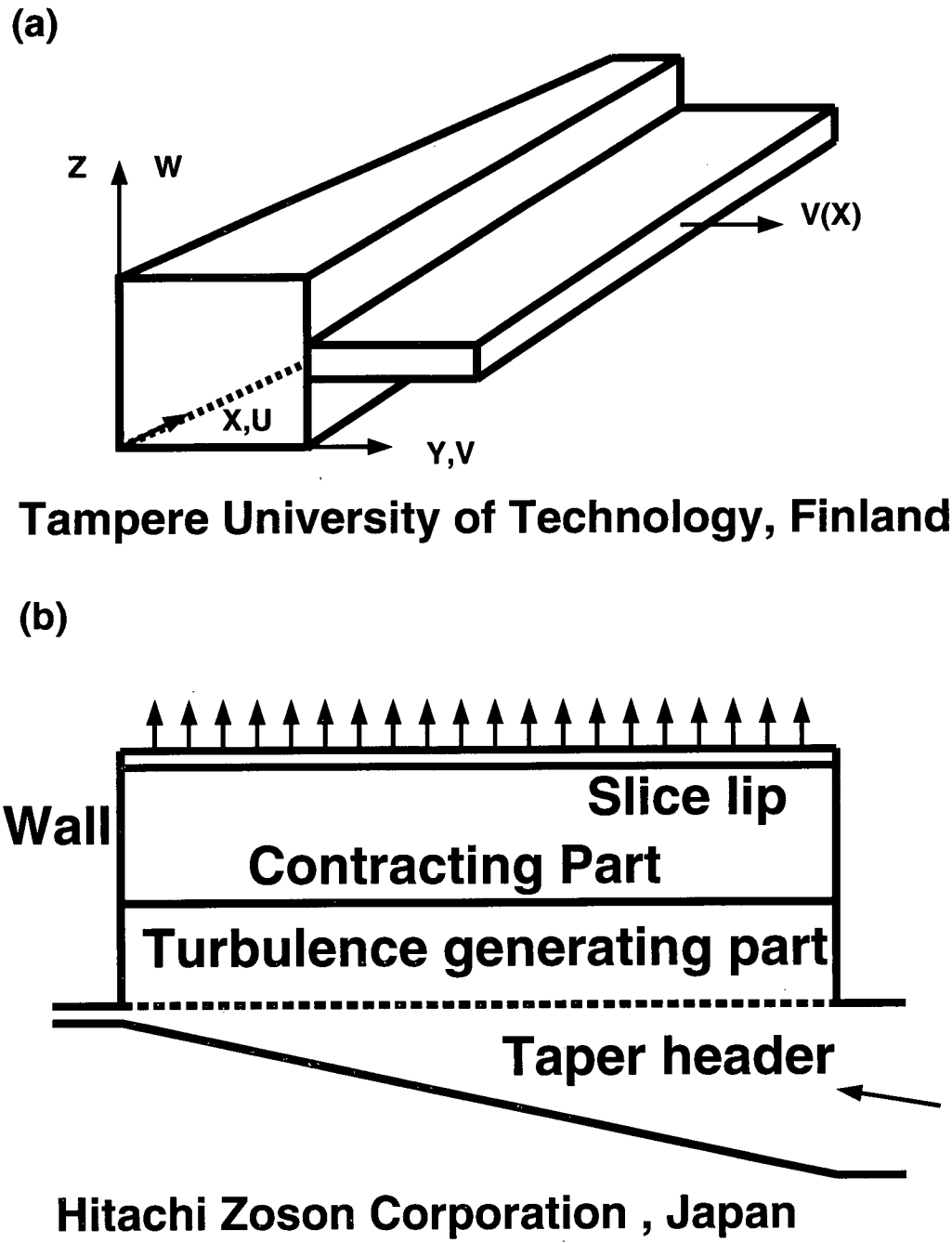

Figure 1.3: Illustration of previous numerical studies

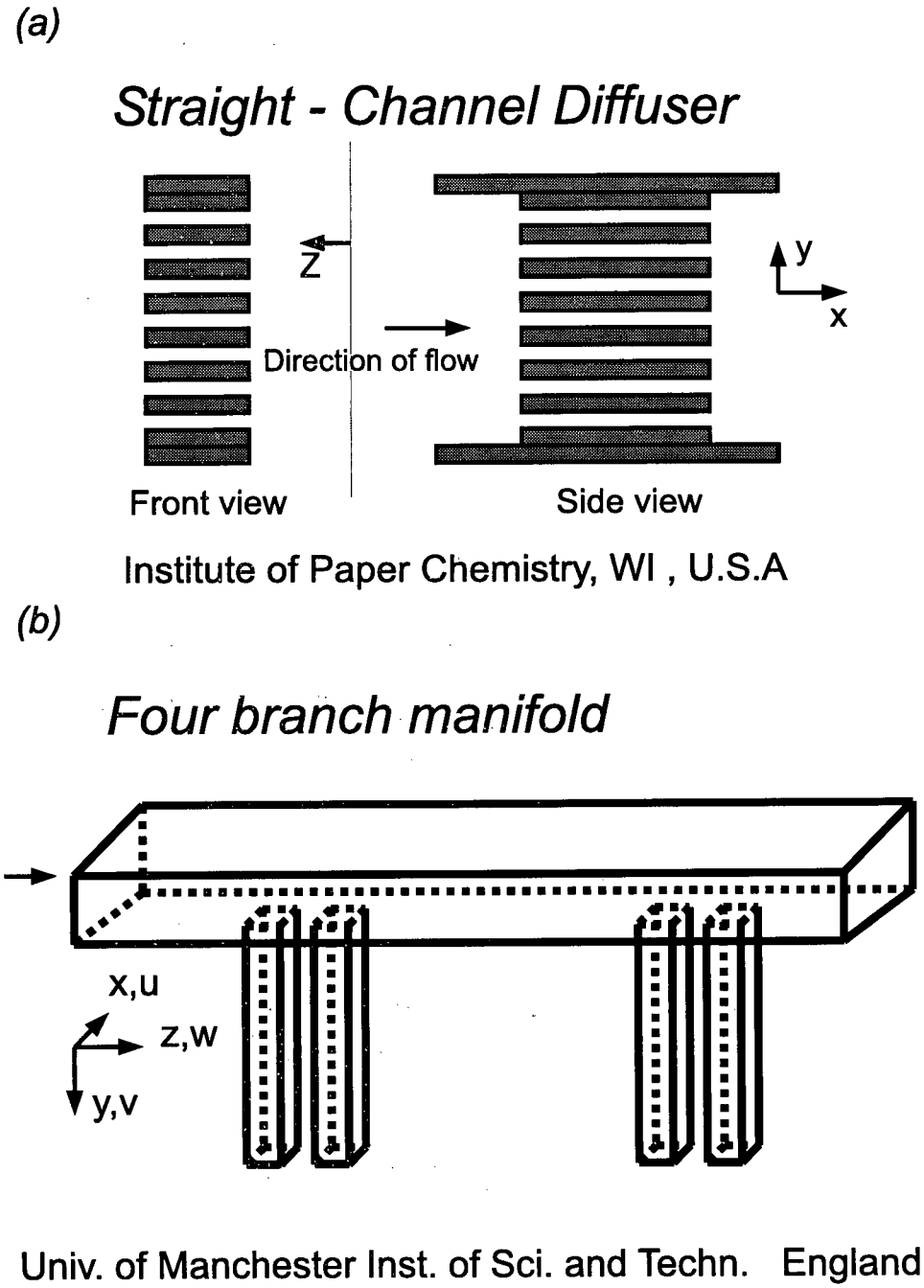

Figure 1.4: Illustration of previous numerical studies

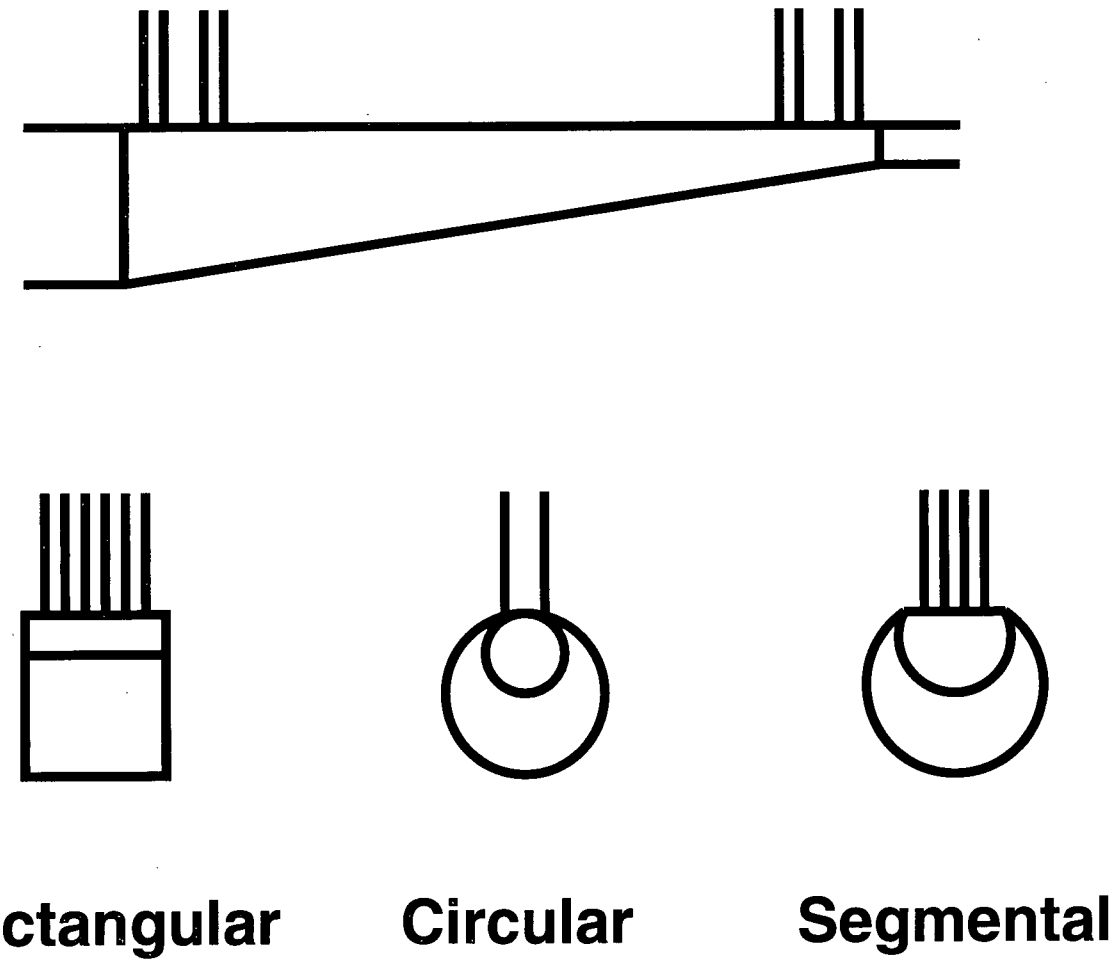

Figure 1.5: Illustration of manifold cross sectional configurations

Chapter 2

Validation of the Computational Method

In this chapter, the performance of the numerical method for simulating manifold type dividing and combining flow is investigated. Two examples are given, one is the flow inside a manifold in a liquid cooling module for electronic packaging, the other is the turbulent flow in a pipe junction having application to engine inlet manifolds. Comparisons with available experimental and numerical results show that the present solution method is reliable.

2.1 Flow in Liquid Cooling Module Manifolds for Electronic Packaging

Manifolds in liquid cooling modules for electronic packaging are used to divide a main fluid stream into several small streams as well as to combine several small streams into a large stream. These manifolds are classified by flow directions into parallel and reverse flow manifolds. In the parallel flow manifold, the flow directions in the dividing and combining header are the same, whereas the flow in the reverse flow manifold are in opposite directions. This problem was chosen because it has a similar manifold dividing and combining flow characteristics as a headbox. The objective of a manifold design is to obtain a uniform flow distribution. Achieving this objective is especially important in the manifold of a liquid cooling module for electronic packaging because local hot spots can significantly reduce the reliability of a system.

Recently, Choi *et al* (1993) numerically studied the effect of the area ratio, the

Reynolds number, and the width ratio on the flow distribution in manifolds of a liquid cooling module for electronic packaging. This geometry was adopted for the present validation study. The parallel manifold has a rectangular header and eight channels of uniform width separated by thin baffles, as shown in Figure 2.1. The same inlet Reynolds number of 50 is used to simulate this two-dimensional and steady laminar flow. A uniform inlet velocity profile assumed. The property values of water at 20^o are used.

The grid for this model is illustrated in Figure 2.2 and was generated by using a multiblock algebraic grid method. Figure 2.3 shows the simulated velocity vectors, streamlines and pressure contours.

The predicted percent flow rate in each channel together with the results obtained by Choi *et al* (1993), is compared in Figure 2.4, where good agreement can be seen. Figures 2.5 and 2.6 show the v-component velocities at the channel entrance (*i.e.* at $y = D$). The results of the computation agrees well with the experimental results of choi *et al.*

2.2 Turbulent Flow in a Pipe Junction Representing an Engine Inlet Manifold

This problem was chosen because experimental and numerical data for the dividing turbulent flows encounted in inlet manifolds are available. It has been realized that this configuration of the inlet manifold has a large effect on the performance of an internal combustion engine. There is an increasing need to further understand the complex fluid-dynamic processes in manifolds to optimize engine geometric design parameters. Recently, Fu *et al* (1992) conducted an experimental and numerical investigation of the flow in an internal combustion engine inlet manifold. The flow in a single-branch manifold was simulated using the $k - \epsilon$ model of turbulence. Steady and incompressible flow characteristics are assumed.

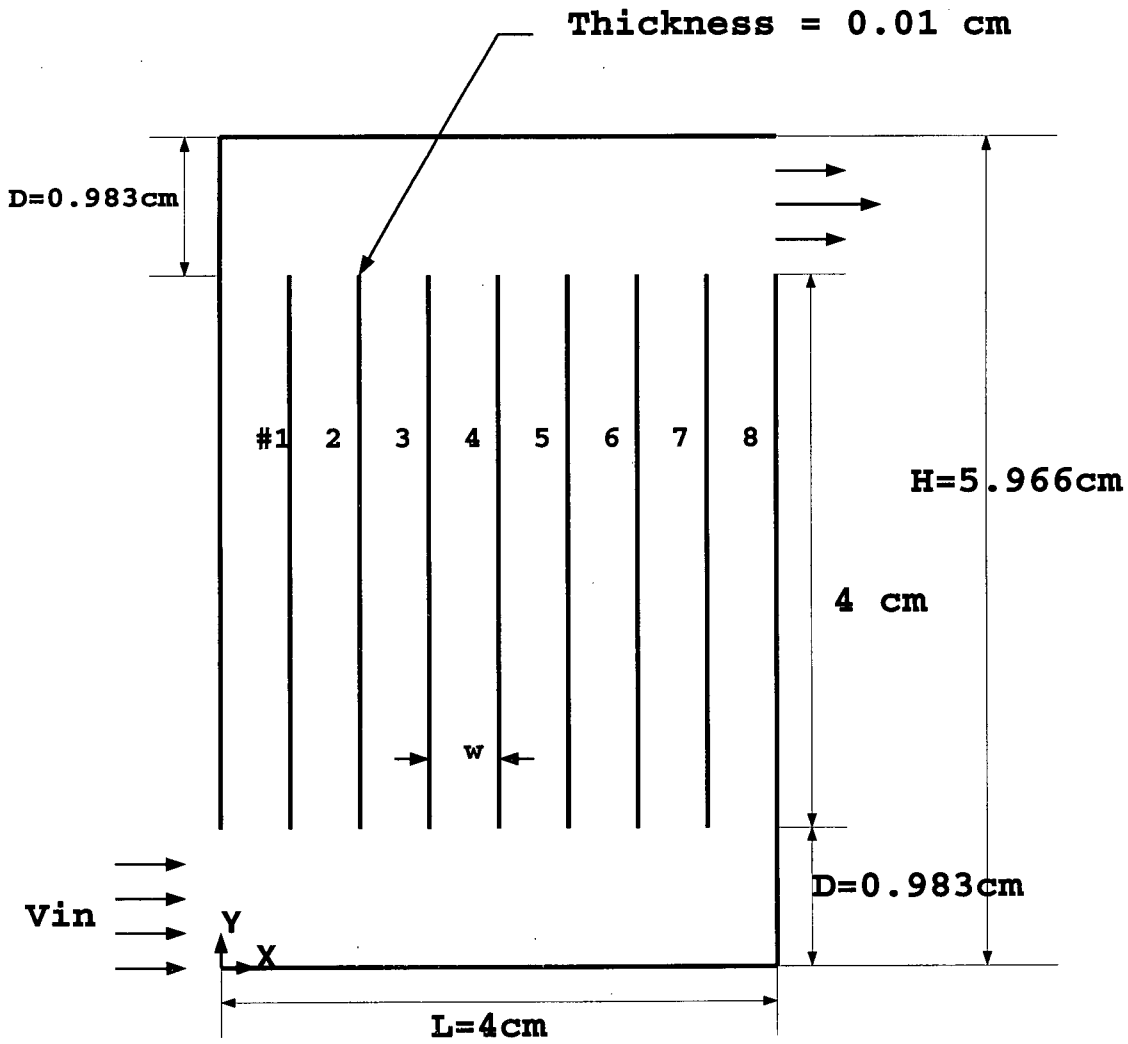

Figure 2.1: Illustration of a parallel manifold in liquid cooling module for electronic packaging

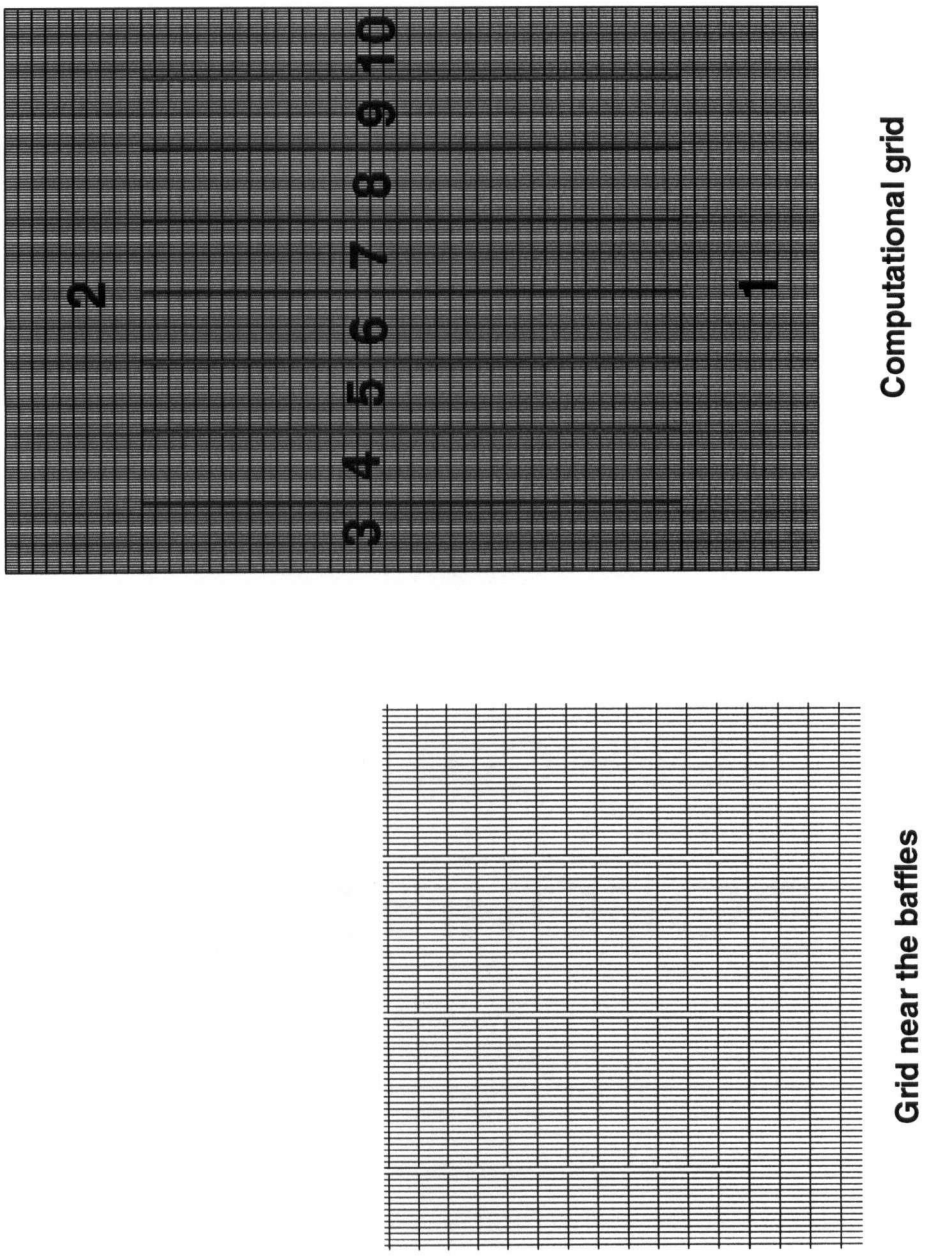

Figure 2.2: Computational grid for the parallel manifold

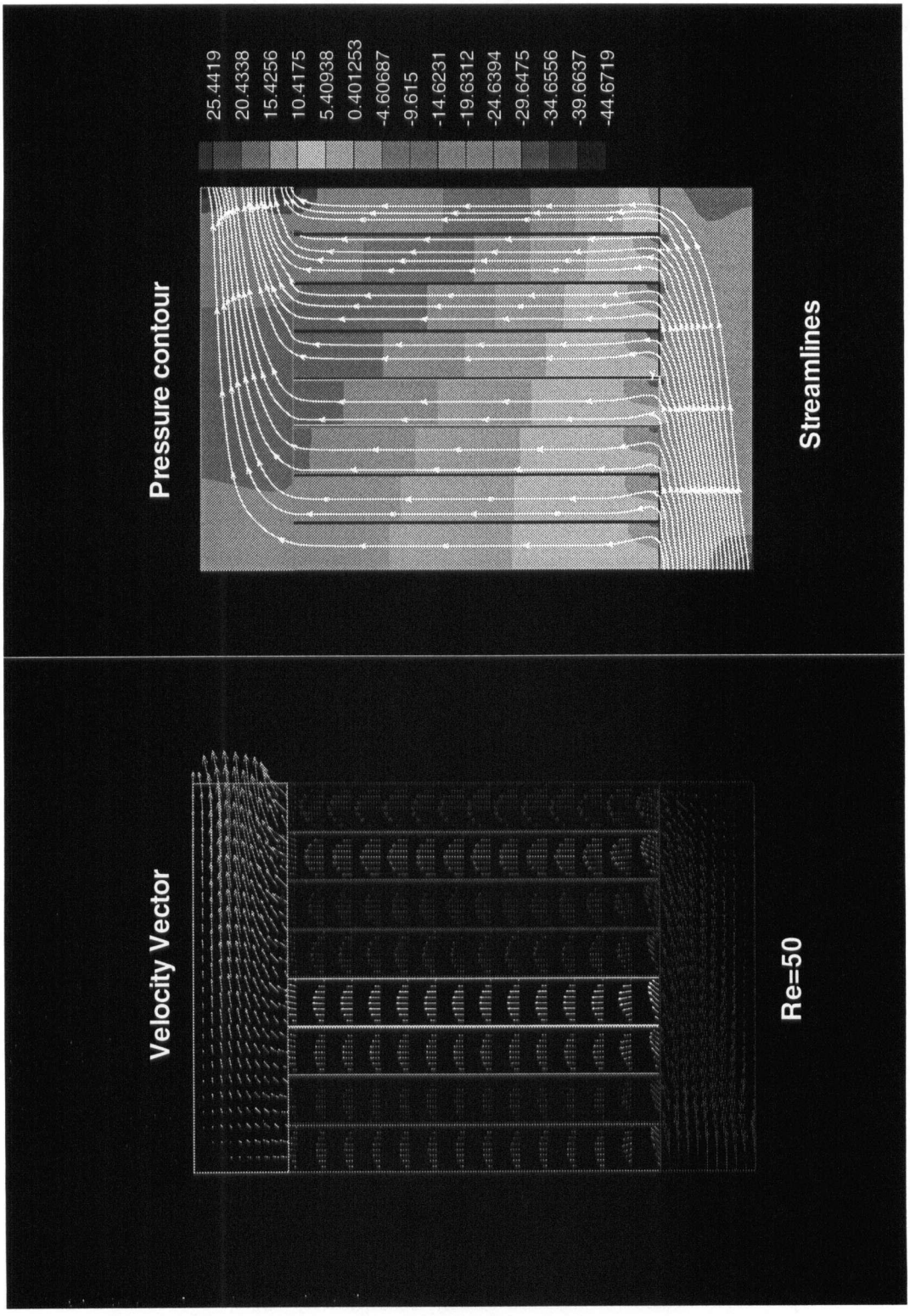

Figure 2.3: Calculated velocity vector and pressure contour for the parallel manifold

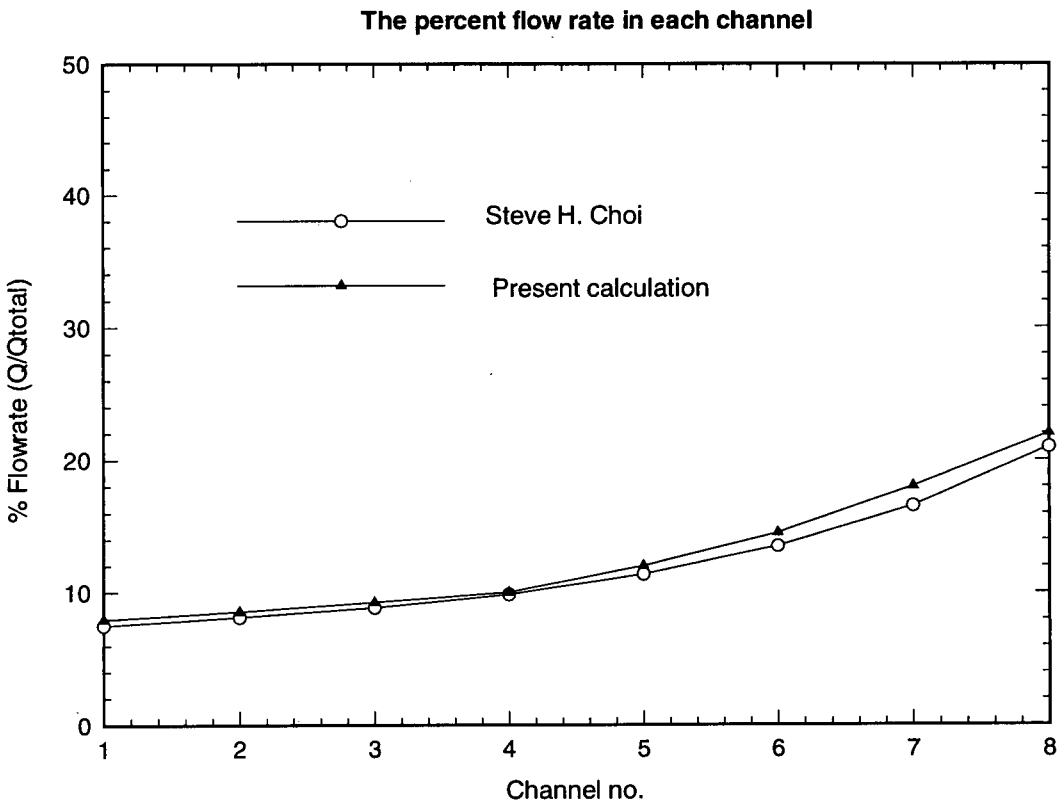

Figure 2.4: Percent flow rate in each channel as numbered in Figure 3.1

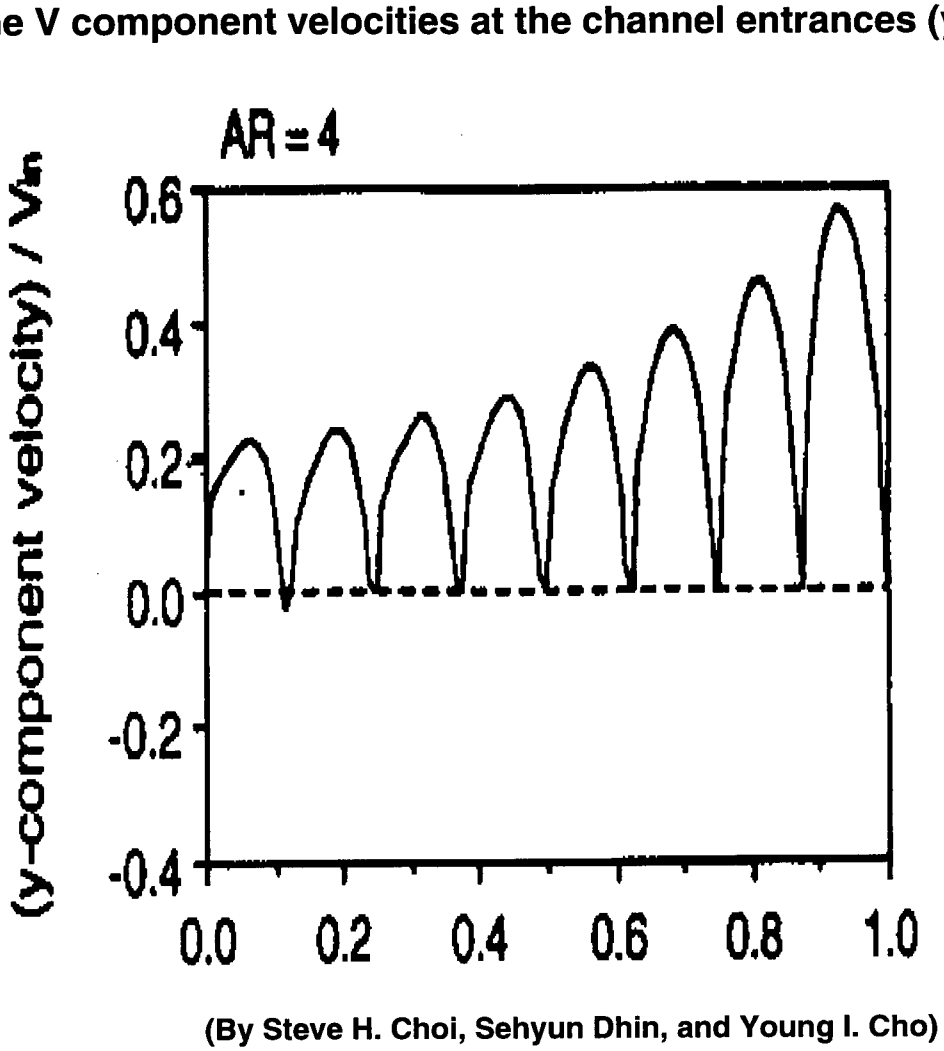

Figure 2.5: V-component velocities at the channel entrance

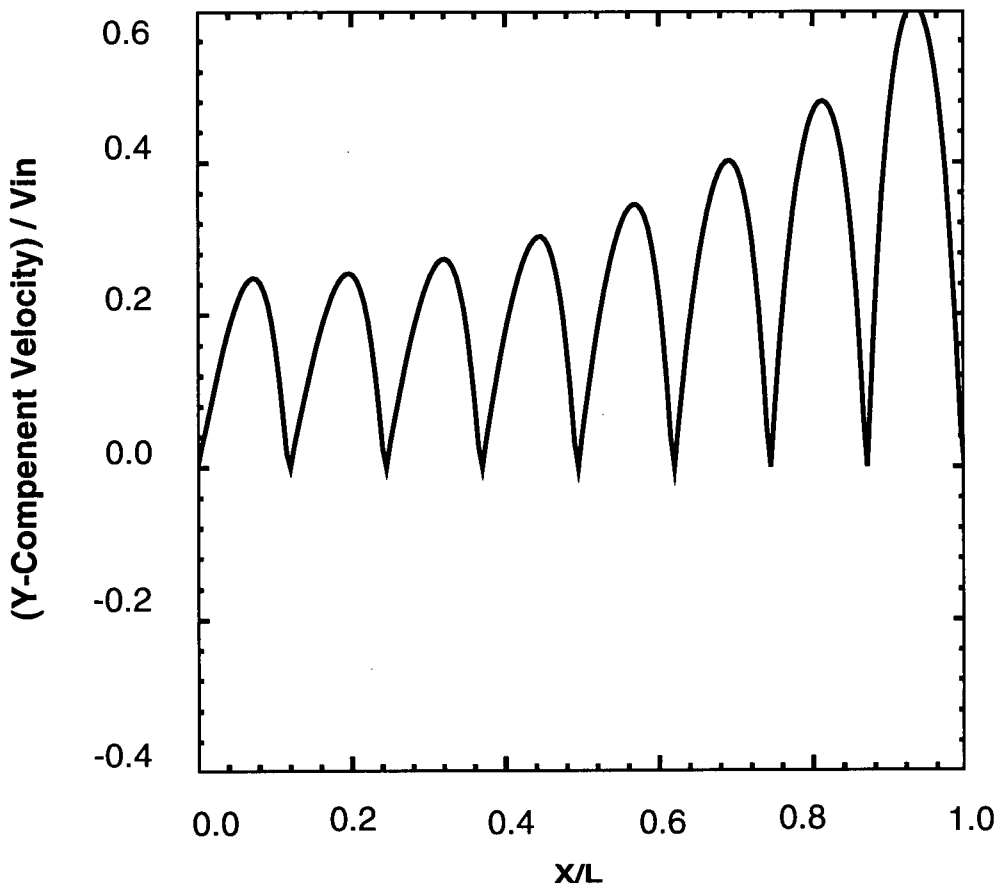

Figure 2.6: V-component velocities at the channel entrance

The flow domain is sketched in Figure 2.7 which shows a T-junction with a duct to branch area ratio of 2.87. The flow Reynolds number based on the bulk velocity at the inlet of the duct and the hydraulic diameter of the duct is $60,000$. Water is used as the working fluid. The multi-block computational grid is plotted in Figure 2.8. Only half of the domain is simulated because the geometry is symmetric about the center plane. Figure 2.9 shows the velocity vector in the plane of symmetry. For these results the bulk velocity and flow rate of the duct inlet are $1.27m/s$ and $3.82mm/s$ respectively, and the branch-main duct flow ratio is 11.6 percent.

The predicted cross-stream motions at different locations together with the results of Fu *et al* are compared in Figure 2.10 and Figure 2.11, respectively. Although there are some discrepancies, the overall agreement is acceptable . A secondary flow is generated in cross- stream planes in the main duct downstream of the interface due to the impingement of the cross-stream flow on the wall.

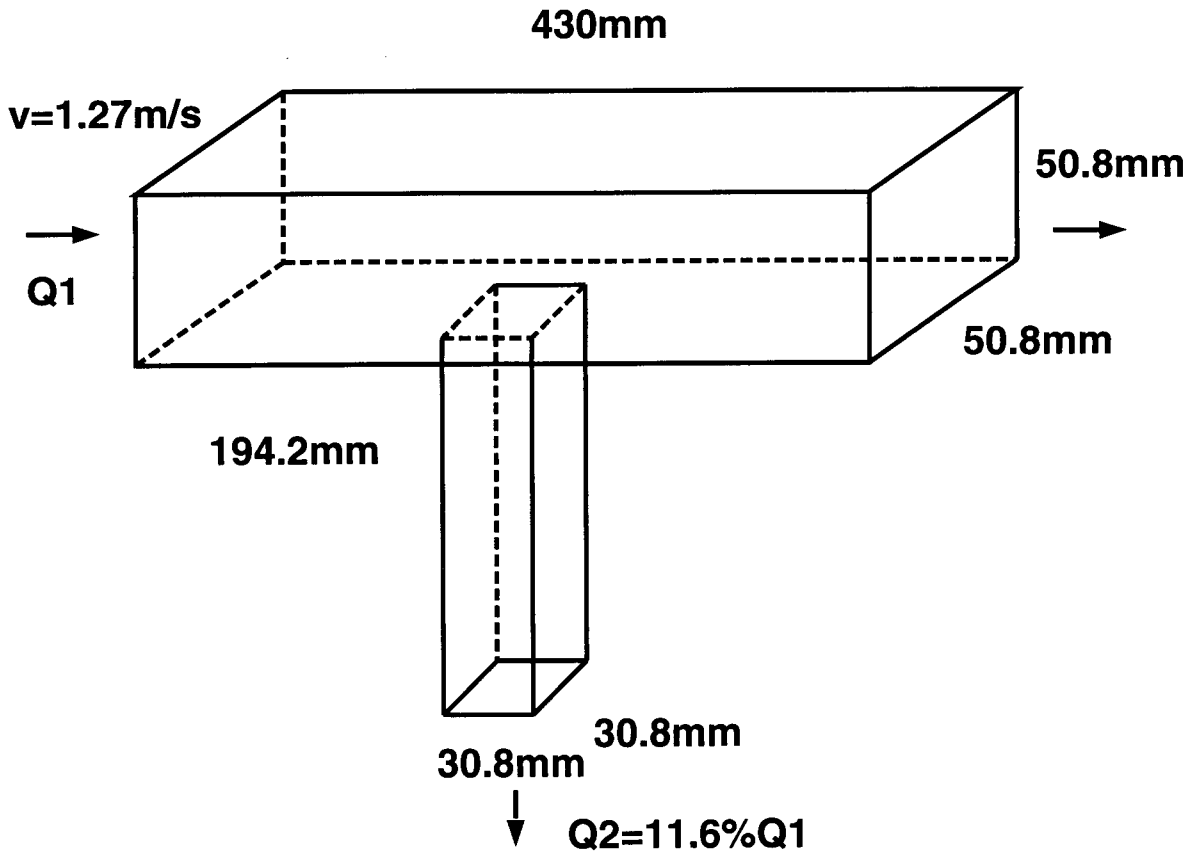

Figure 2.7: Illustration of a T-junction flow domain

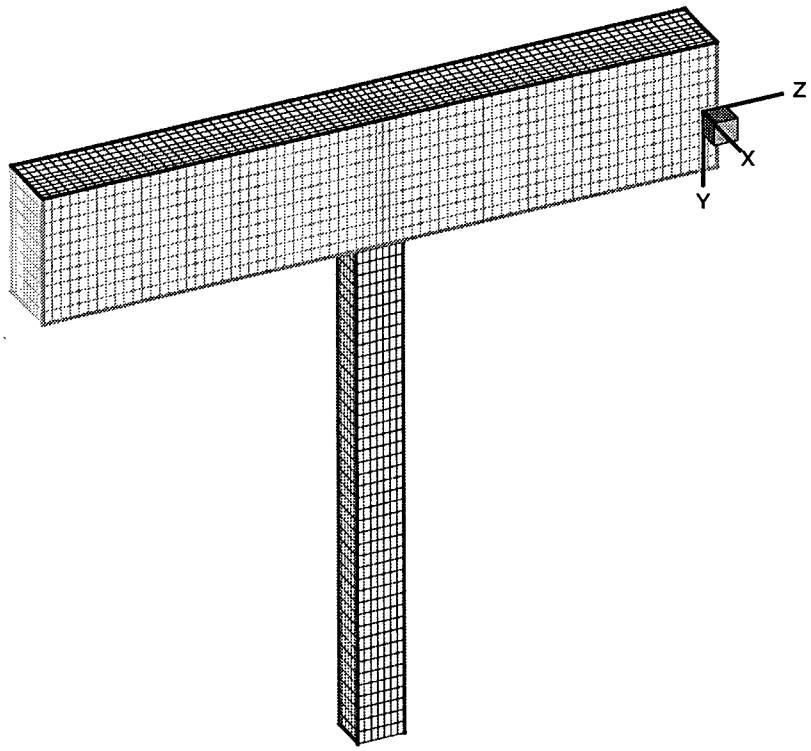

Figure 2.8: Computational grid for the T-junction flow domain

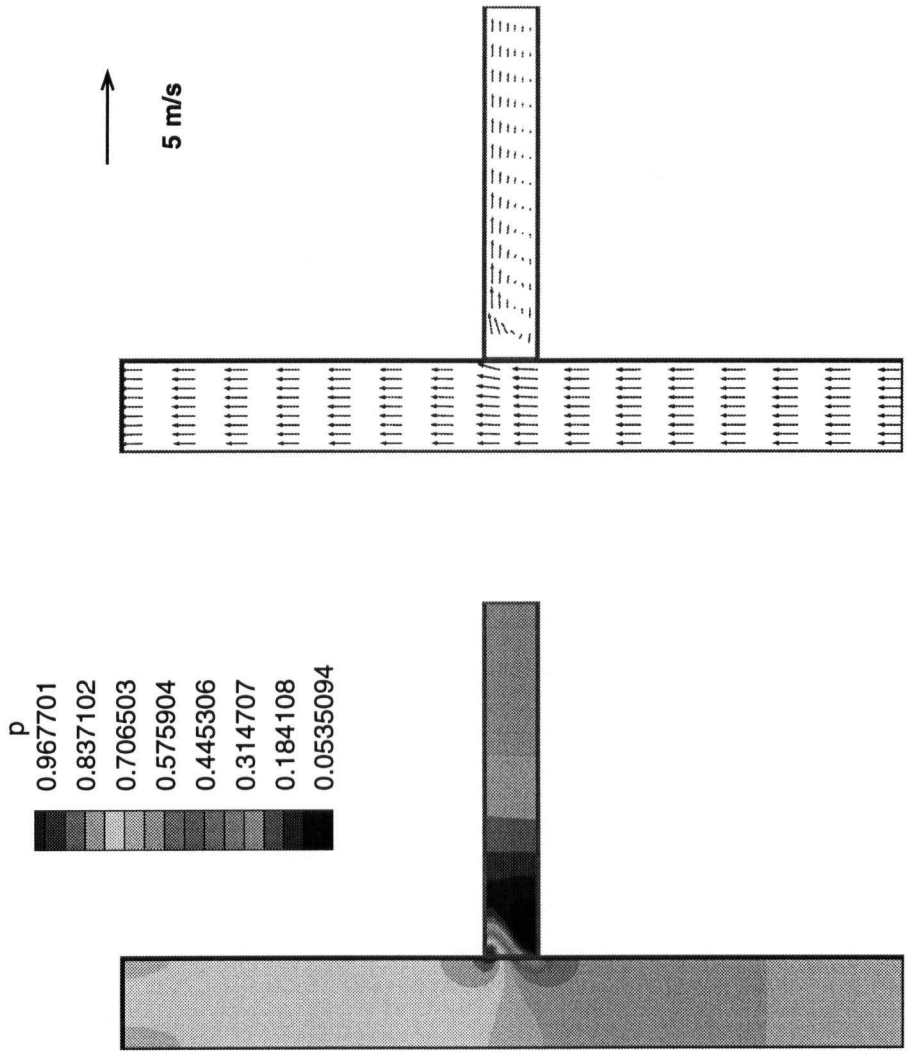

Figure 2.9: Pressure contour and velocity vector in the plane of symmetry for the T-junction flow domain

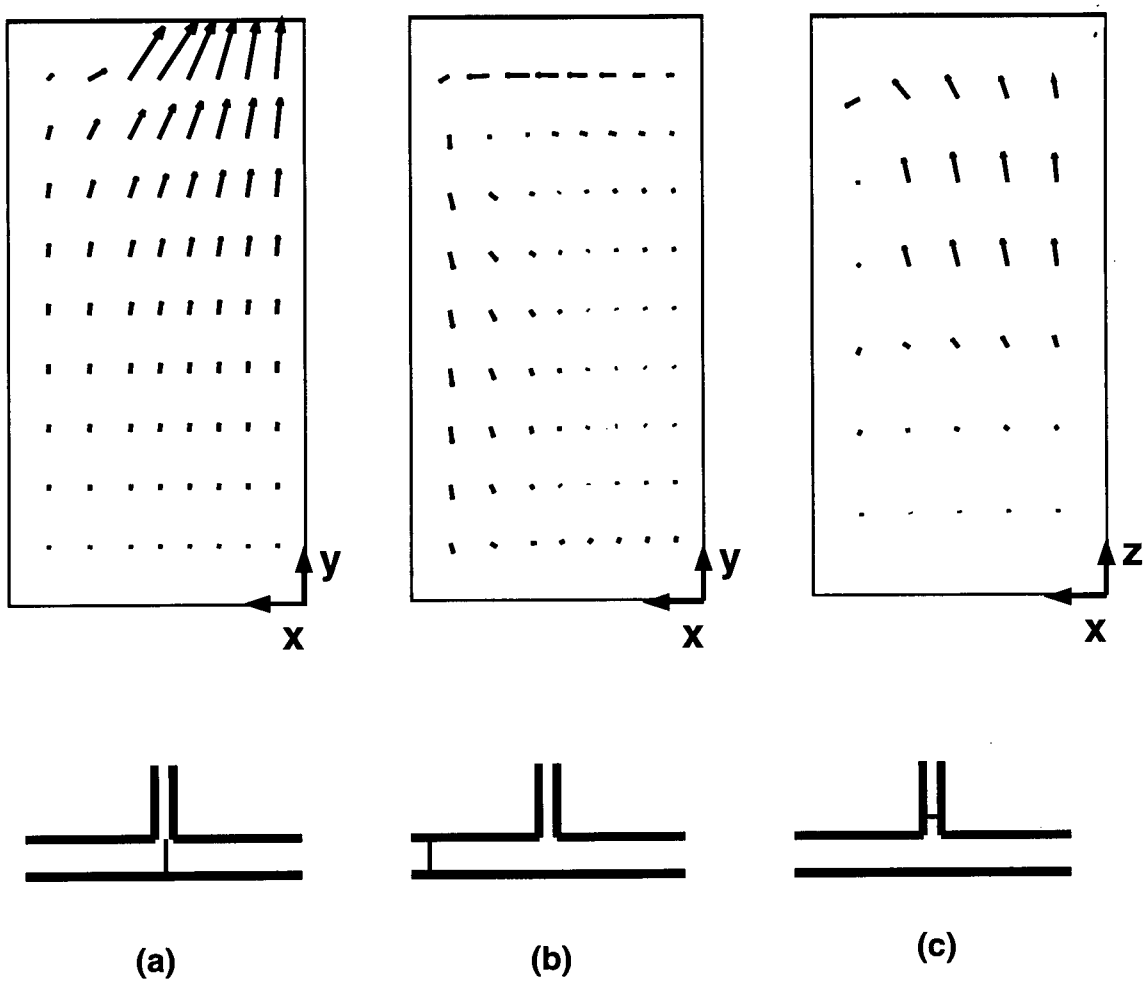

Figure 2.10: Cross-stream motions at three different locations. Location of cross sections are shown in the sketches below each vector plot

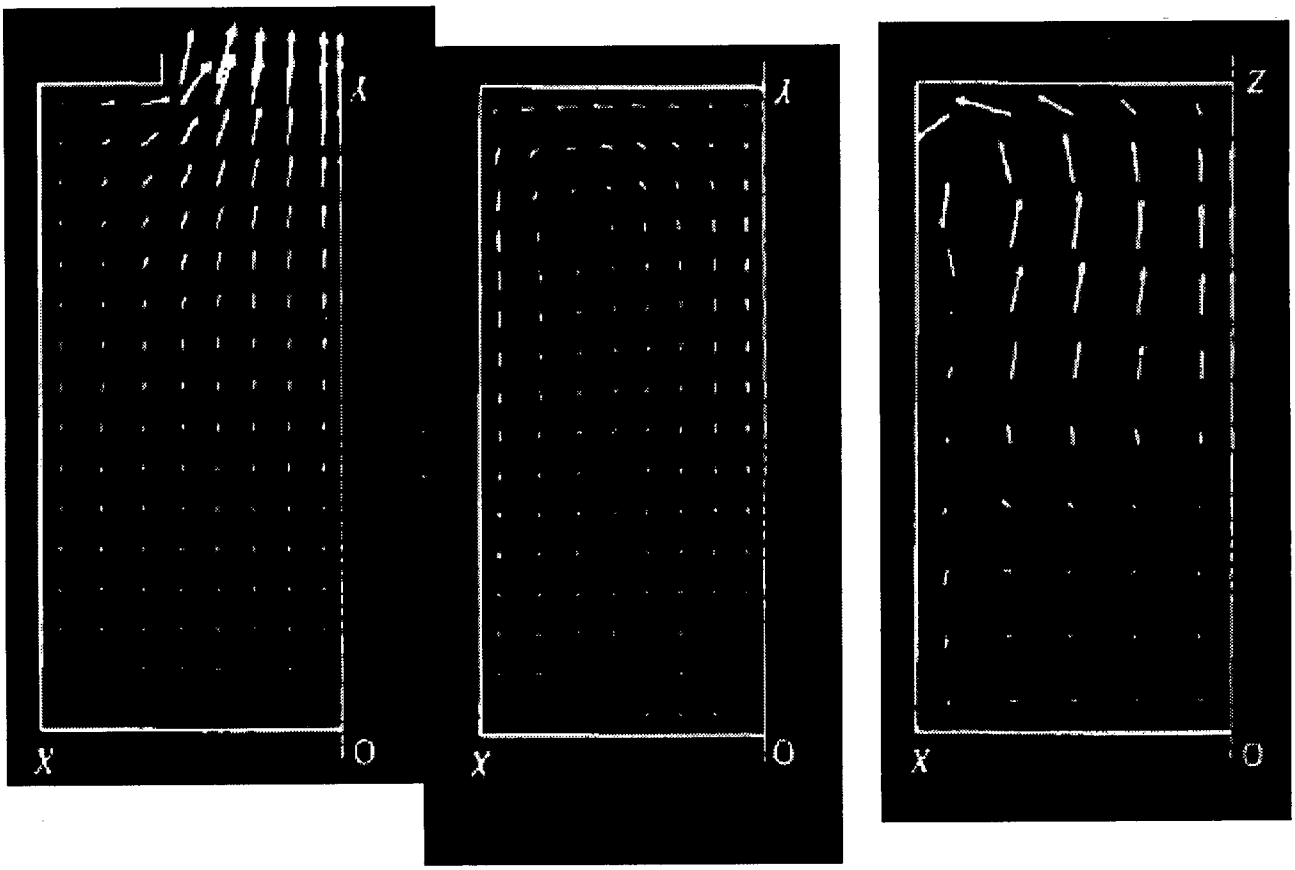

Figure 2.11: Cross-stream motions at three different locations computed by Fu *et al* ,1992. Cross sections are located as shown in Figure 2.10

Chapter 3

Prediction of the Flow Distribution in a Flow Diffuser

Computational results are presented for a Canfor headbox flow diffuser. This flow diffuser consists of a tapered rectangular duct and a bank of diffuser tubes. The computational methods described in previous chapters are used to simulate the flow in this complex geometry. The computational domain is segmented into a number of sub-domains. A block-structured, non-orthogonal grid is used to represent the curved header as well as the diffuser tubes. Computations are carried out for several different simplified models.

3.1 Problem Description

The headbox manifold under consideration is that of the Canfor flow diffuser, as shown in Figure 3.1. There are 80 tubes in the spanwise direction and 7 rows, as shown in Figure 3.2. The 3D view of the manifold is shown in Figure 3.3. The circular inlet cross section of the manifold is $0.9m$ in diameter. Individual tube inlet diameter in the tube bank is around $0.02m$.

Taking the advantage of the flow symmetry about the center plane, computations are performed for half of the physical domain. The computational domain includes a main flow region, 80 tubes in each of the first three rows, and 80 half tubes in the fourth row. The main flow region extends upstream and downstream (in the positive x-direction), as shown in Figure 3.1(a).

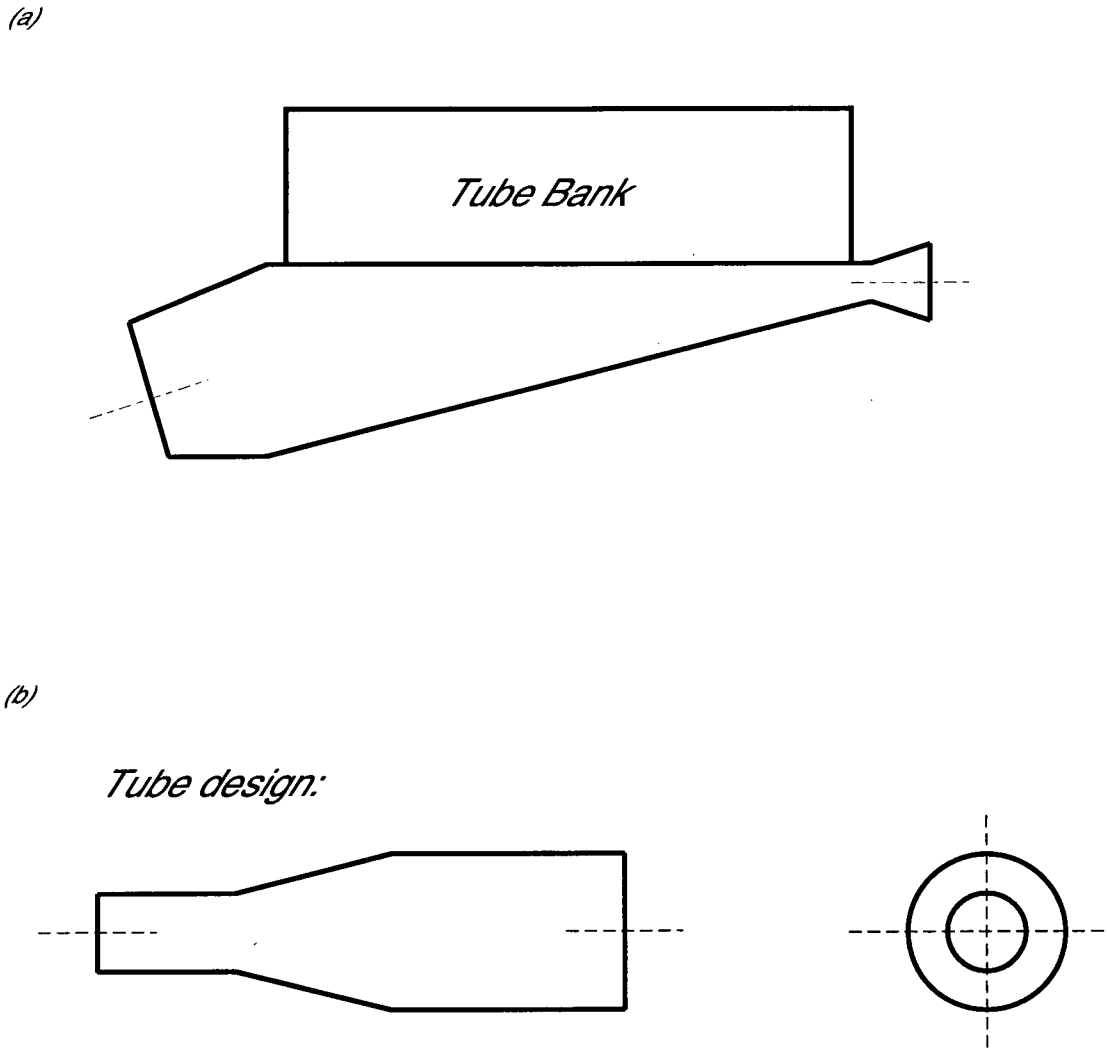

Figure 3.1: Illustration of the Canfor headbox flow diffuser (a) side view of the whole manifold (b) side view of the diffuser tube

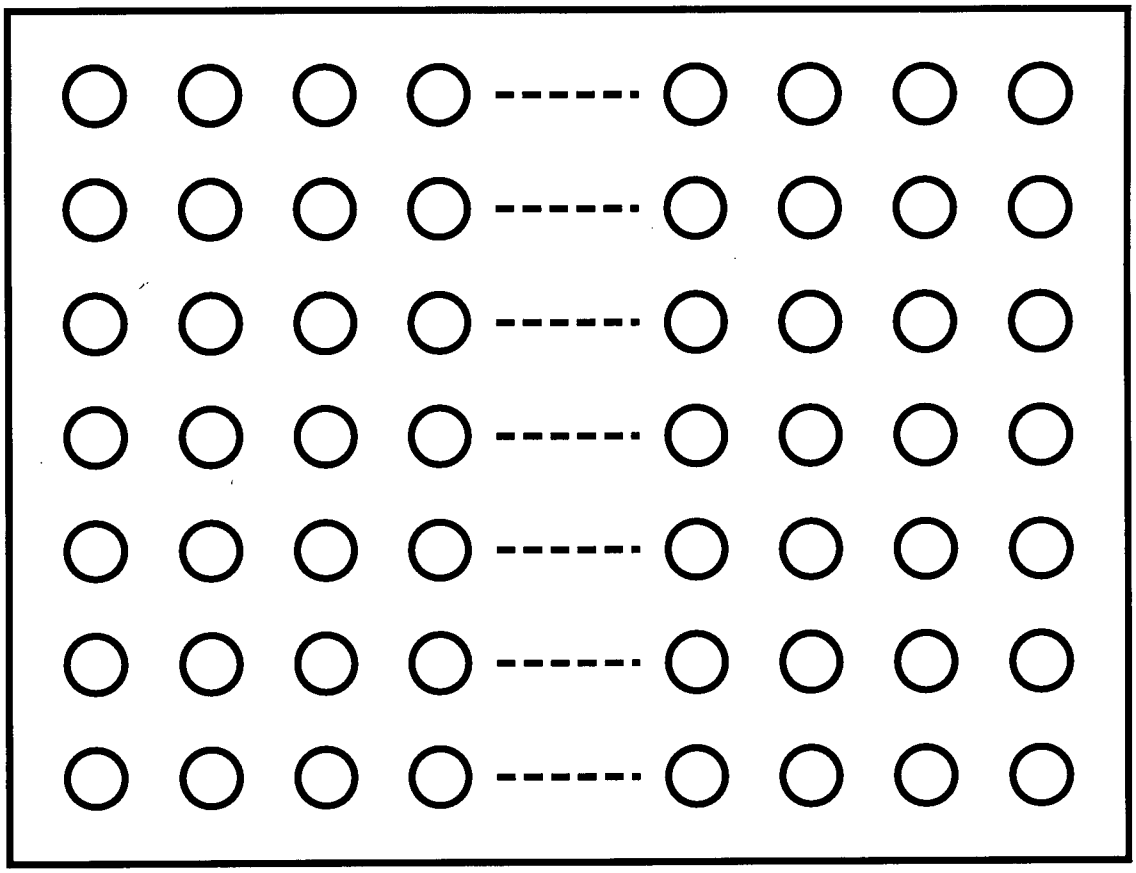

Figure 3.2: Illustration of the top view of the tube bank

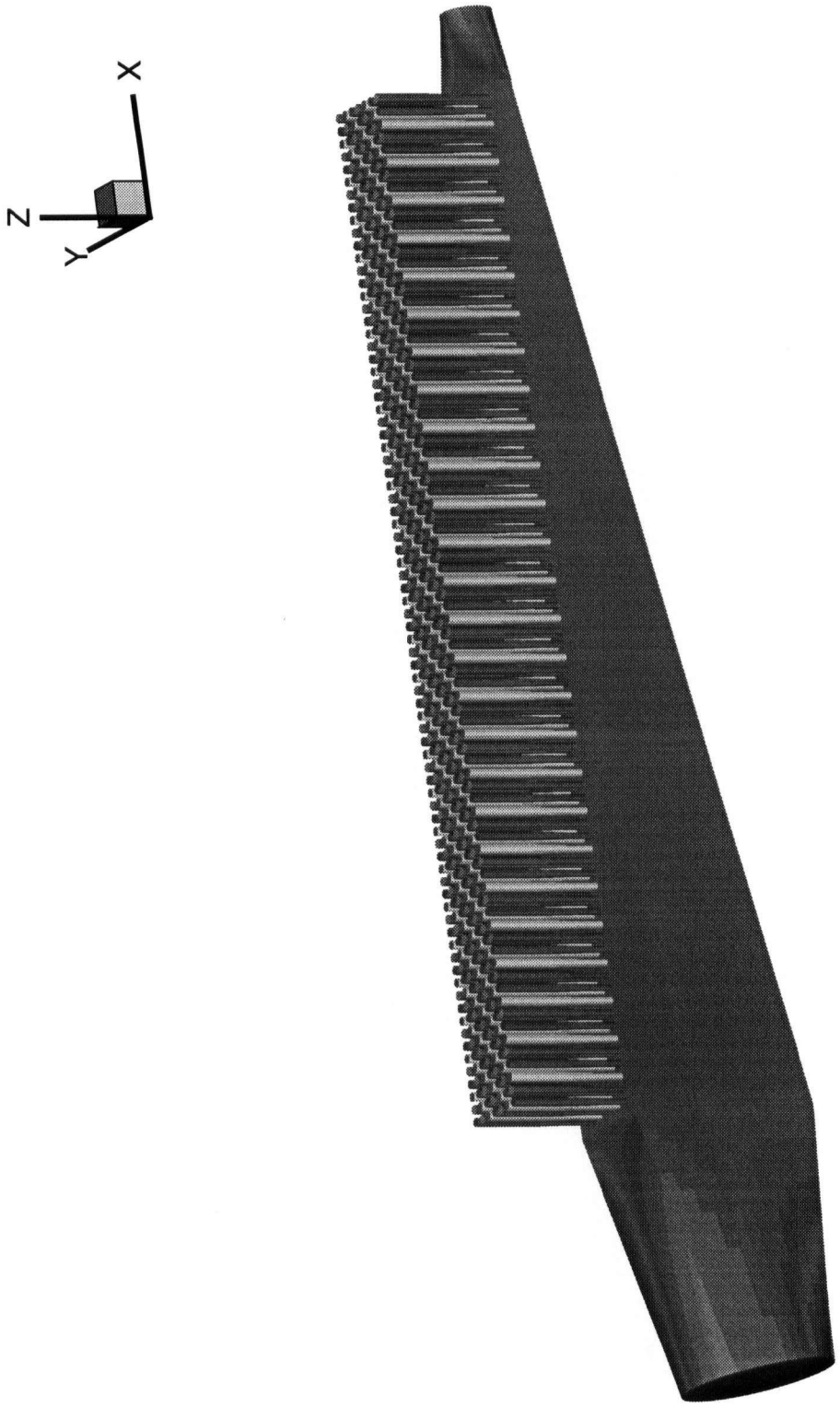

Figure 3.3: 3D view of the Canfor manifold

3.2 Computational Grids

The grid was generated using the method described earlier. The computational domain is segmented into a main flow subdomain and 320 diffuser flow subdomains. In order to obtain a continuous grid at the interface, rectangular grids are used for the diffuser tubes instead of cylindrical grids which have a singular line at the center (see appendix C). The generated grid is shown in Figure 3.4. The grid used for the present study contains $377 \times 18 \times 13$ nodes in the main flow region. Due to computer limitations, only 3×3 nodes per tube cross section are used for the real geometry simulation since there is a large number of tubes in the x direction which could give rise to too many nodes to be solved. Much finer grids are used for the diffuser tube in simplified models which have fewer tubes.

3.3 Solution Procedure

In principle the fluid flow in the manifold could be simulated in its actual three dimensional geometry. Two problems exist in this approach. First, the generation of the grid would be quite laborious. Secondly, the manifold tube bank may consist of hundreds of tubes each tube requiring several hundreds of cells. Those are the main reasons why there is no direct simulation for the manifold in the literature. In the present study, the grid generation problem is solved by using the combination of elliptic grid generation and algebraic grid generation methods. Three by three grid nodes are used in the tube cross section which results in 168,858 cells for the complete Canfor manifold. Finer grids for the simulation of the tube cross section like 5×5 grid nodes would result in about one million cells for the whole Canfor manifold. This has too many unknowns to be solved due to computer memory limitations.

Since the direct simulation of the manifold is limited to a coarse grid, fewer tube

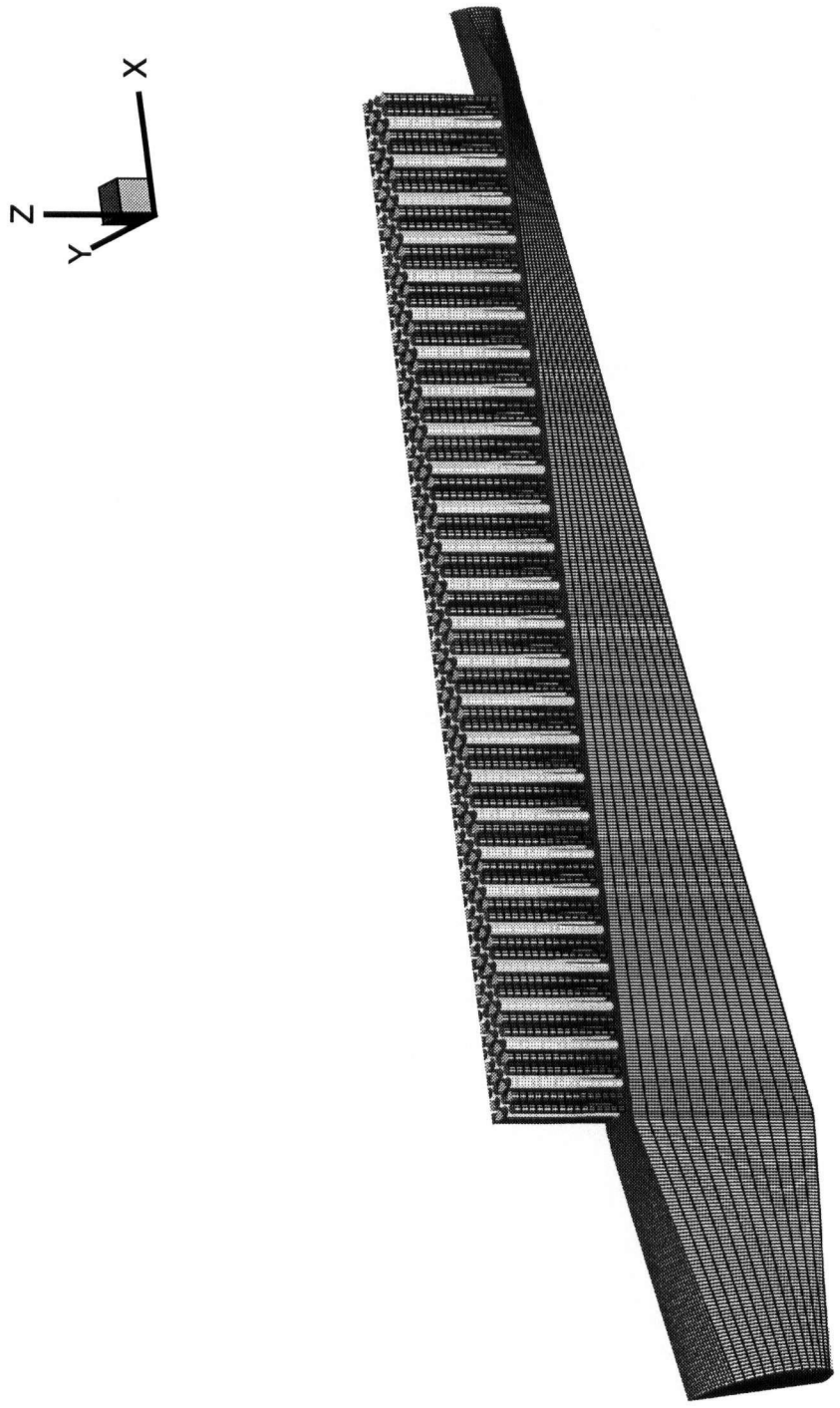

Figure 3.4: Grid generated for the present calculation containing $377 \times 18 \times 13$ grid nodes in the main flow region and $3 \times 3 \times 30$ grid nodes for each tube

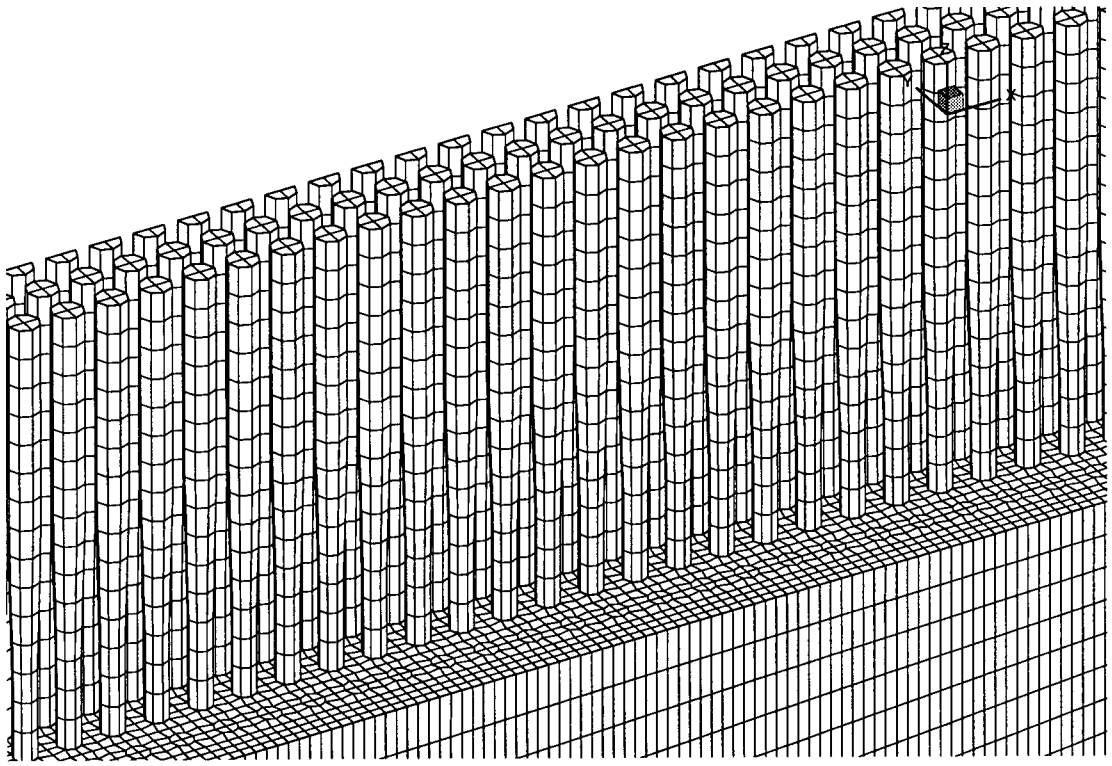

Figure 3.5: Computational grid near the interface between the plenum and the tube bank

models with the same open area are adopted and tested with finer grids. The same coarse grid level is used for direct simulation with a model using fewer tubes and the results are compared to validate the accuracy of the fewer tube model. Much finer grids are also used for those fewer tube models to achieve high resolution results.

3.4 Boundary Conditions

Four types of boundary conditions are used: inlet, outlet, wall and no-flux. The treatment of boundary conditions on each boundary can be described as follows:

- Inlet:

  The inlet plane of the mainstream (the west plane of the main flow region) where all the dependent variables except pressure are prescribed is located $1.52m$ upstream from the tapered rectangular duct. The mean velocity is taken as $U_\infty = 1.088\ m/s$ as characteristic of the operational velocity of this manifold. The turbulent energy and turbulent dissipation were evaluated using the following formulas:

  $$k = 1.5U^2(u/U)^2, \qquad \epsilon = C_\mu^{\frac{3}{4}} k^{\frac{3}{2}}/l \tag{3.1}$$

  where u/U is the turbulence intensity and l is the turbulence length scale. The turbulence intensity is assigned a value of $u/U = 0.5\%$ and the turbulence dissipation is calculated based on a length scale equal to the diameter D of the inlet. Since the turbulence intensity is small at the inlet, these assumptions should not affect the results significantly.

- Wall:

  The wall is assumed to be impermeable with zero tangential velocity. The standard 'wall function' described by Launder and Spalding (1974) is used.

- No-Flux Condition:

  The north boundary located at a distance $0.32m$ in the y - direction from the south planes, where the symmetrical plane condition is imposed.

- Outlet :

  Two types of boudary conditions are used for the outlets. One is the zero-gradient condition in the streamwise direction which is imposed for all dependent variables at the outlet boundary. It is sufficiently far downstream to ensure that the flow in the upstream region is not affected by downstream conditions. The second type is the flux boundary condition which is imposed at the large plenum outlet.

3.5 Computational Procedure

Three cases were simulated: 10-tubes, 20-tubes and all tubes. For the 10-tube and 20-tube model, the flow diffuser tube bank is replaced with a number of tubes of large tube diameter. The diameter is large enough to keep the same open area. The length/diameter ratio of the tube is held constant to keep the same pressure loss in each tube. The diameter and length are given by the following relations:

$$\text{(1) for 10 tubes, then } D_{10} = d \times \sqrt{56} \text{ and } L_{10} = l \times \sqrt{56} \text{ and}$$

$$\text{(2) for 20 tubes, then } D_{20} = d \times \sqrt{28} \text{ and } L_{20} = l \times \sqrt{28}.$$

Here d is the bottom diameter of the diffuser tube and l is the tube length.

$2 \times 2 \times 30$, $4 \times 4 \times 30$, $6 \times 6 \times 30$, $8 \times 8 \times 30$, $12 \times 12 \times 30$ and $16 \times 16 \times 30$ cells are used for the diffuser tubes in the computation of the 10-tube model to study grid independence. $2 \times 2 \times 30$, $4 \times 4 \times 30$, $6 \times 6 \times 30$, $8 \times 8 \times 30$ cells are adopted for the 20-tube model calculation. Grid independence is approached for the $6 \times 6 \times 30$ refinement. All grid independence studies are carried out with 8% recirculation rate.

The effect of manifold recirculation rate on the tube outflow uniformity has been studied by using the 10-tube model, Calculations were carried out with high, low and zero recirculation rates of 15%, 8% and 0%.

The non-uniformity of tube outflow was compared for the 10-tube, 20-tube and direct simulation results.

3.6 Results and Discussion

The computational results are presented in this section. It should be mentioned that some of the detailed results are not presented for the complete computational domain for reasons of clarity.

Grid independence was investigated in this study to ensure that sufficient grid points were used to capture the important phenomena governing this turbulent flow problem. Figure 3.6 presents the results of grid independence studies of a 10-tube model and Figure 3.7 shows the different grid refinements used for the present study. It can be seen that the coarse grid with 2×2 and 4×4 for the tube cross section produces significantly non-uniform flow rate distribution when compared with 6×6 for the tube cross section. It was also found that further grid refinement beyond 6×6 did not produce significant changes in the calculated results.

Figure 3.8 shows the computational grid with $6 \times 6 \times 30$ cells for each diffuser tube; the local velocity field in the xz-plane is shown in Figure 3.9.

Figure 3.10 presents results of grid independence studies of a 20-tube model and Figure 3.11 shows the different grid refinement used for the present study. The results show that grid independence is achieved when $6 \times 6 \times 30$ cells or a finer grid is used for each diffuser tube.

Figure 3.12 shows the computational grid with $6 \times 6 \times 30$ cells for each diffuser tube,

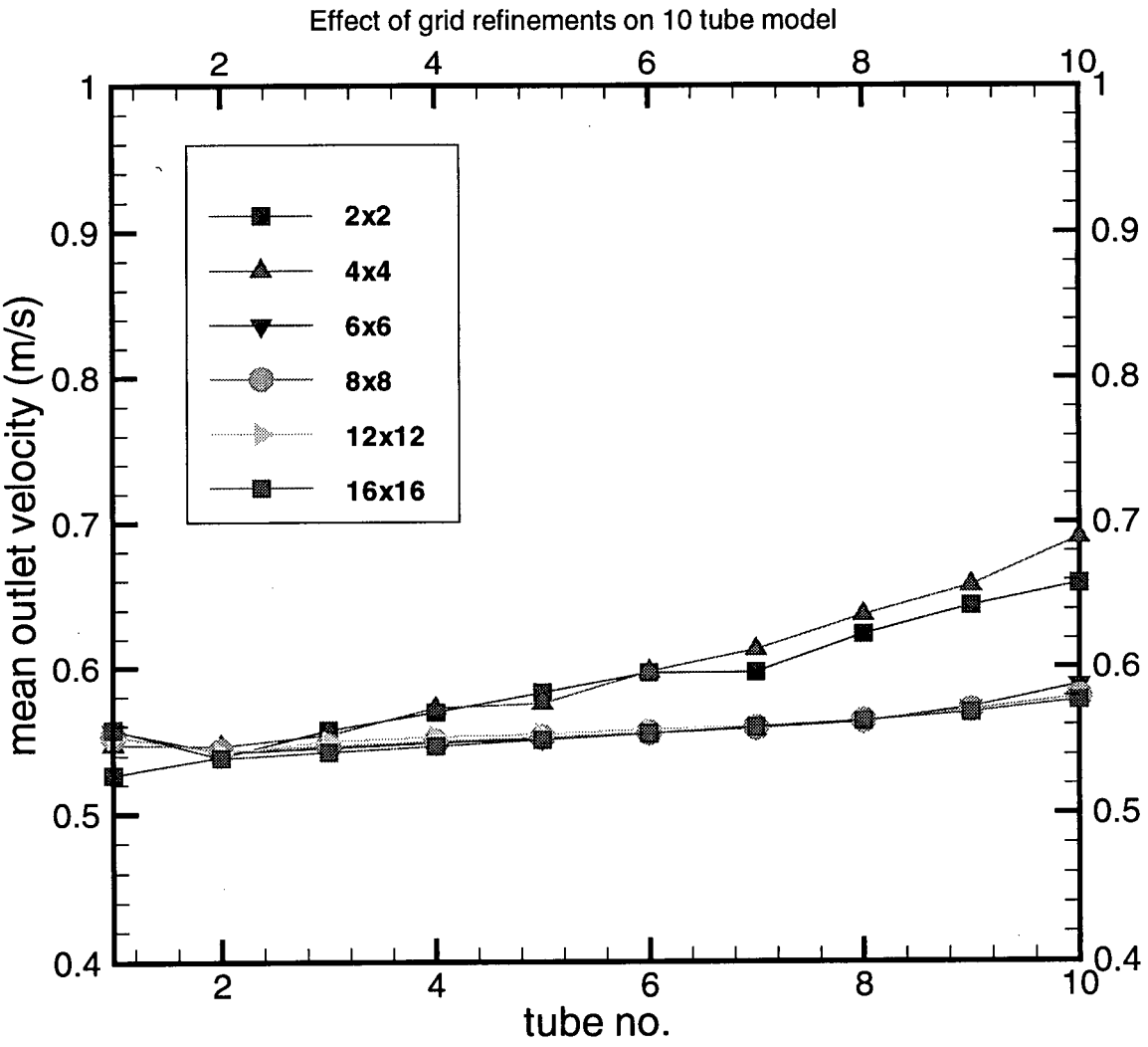

Figure 3.6: Grid independence study of a 10-tube model

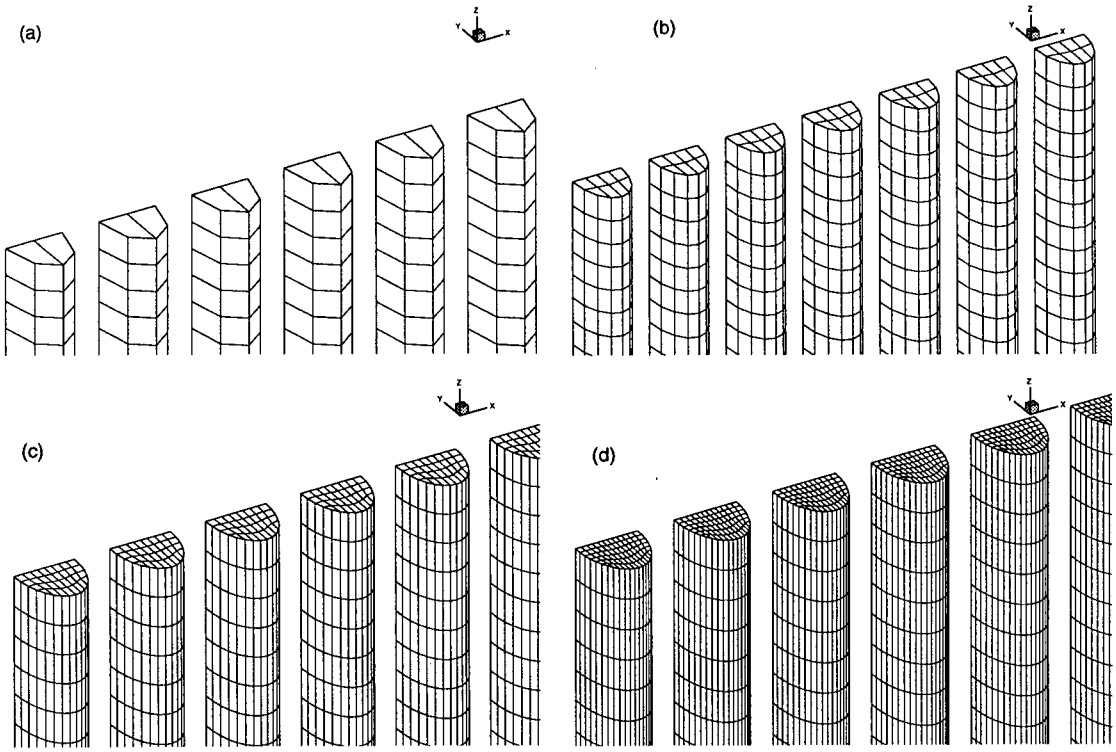

Figure 3.7: Different grid refinement used for 10-tube model study (a) $2 \times 2 \times 30$, (b) $4 \times 4 \times 30$, (c) $8 \times 8 \times 30$, (d) $12 \times 12 \times 30$

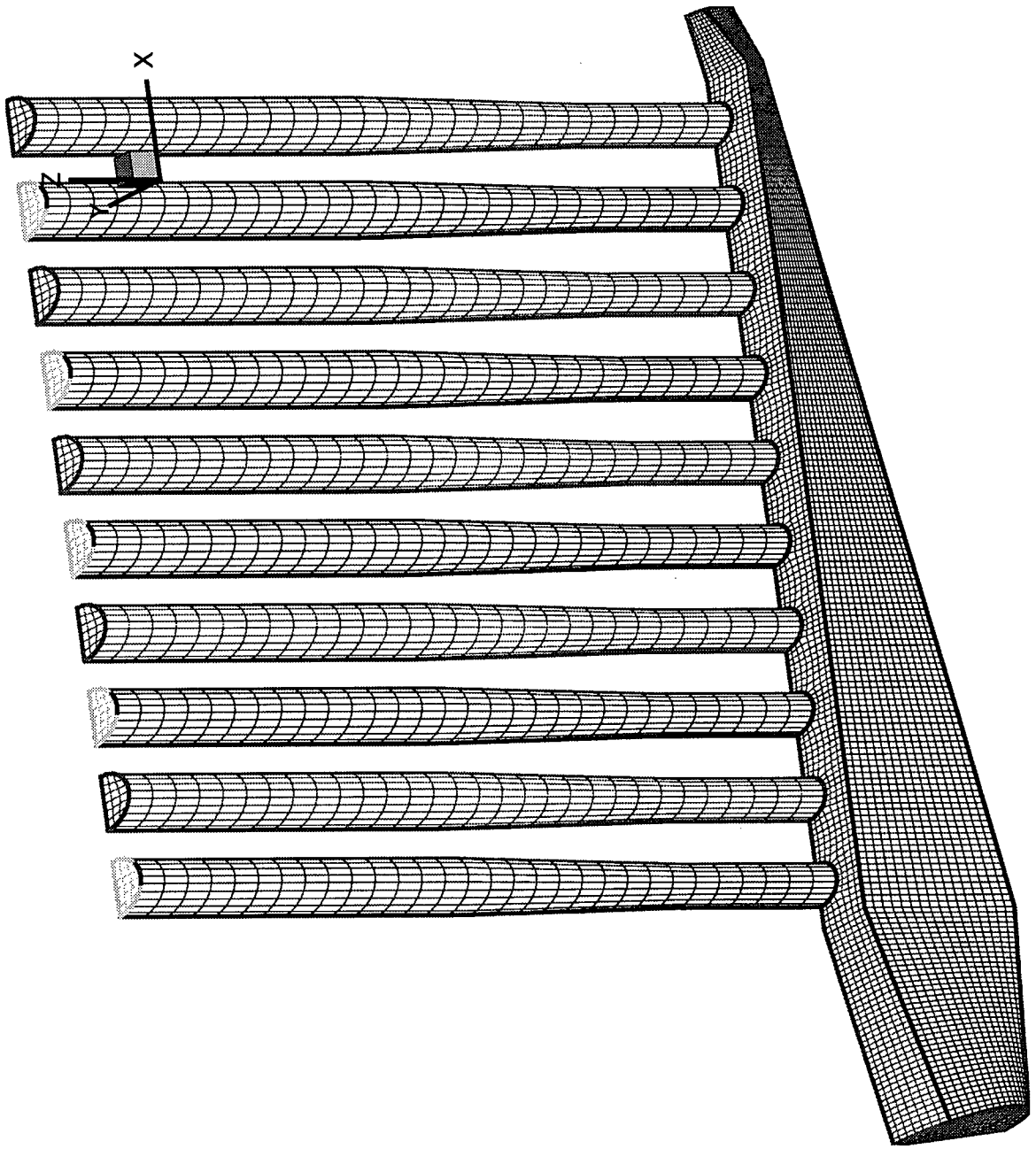

Figure 3.8: Computational grid for the 10-tube model with $6 \times 6 \times 30$ cells for each diffuser tube

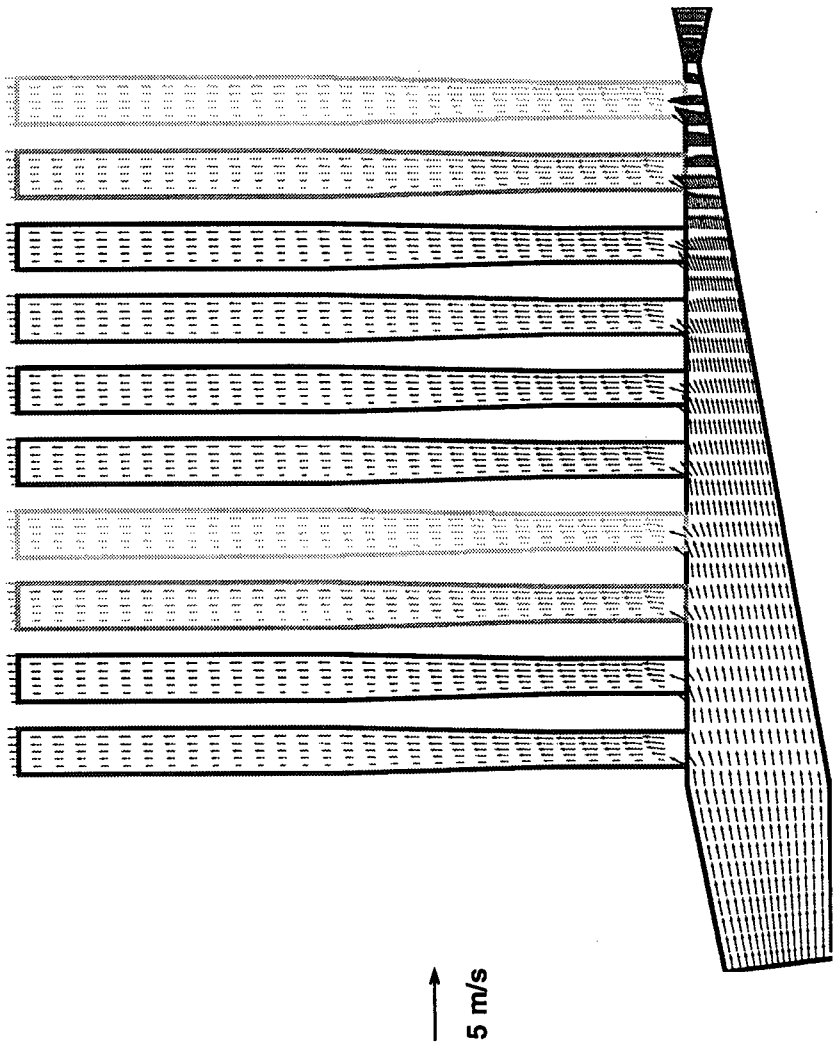

Figure 3.9: Velocity field in the xz-plane

the local velocity field in the xz-plane is shown in Figure 3.13.

Due to computer limitations, only 2×2 cells for each tube cross section have been used to perform the all tube simulation which includes the main domain and 320 subdomains. The same grid refinement was applied to the 10-tube and 20-tube model. Results are shown in Figure 3.14. The results of the all tube simulation and the fewer tube models, when computed on 2×2 grid refinement, are esentially the same. The conclusion is therefore made that the fewer tube models are close representations of the real geometry. Hereafter, the 10 and 20-tube model will be used to investigate the effect of recirculation rate. Non-uniformity of flow in Figure 3.14 is due to the coarse grid which is used. As the grid independence studies shows, more grid refinement is required to capture the large pressure and velocity gradients at each tube entrance.

An essential feature of the tapered manifold flowspreader developed by Mardon (1971) and his colleagues is the recirculation of part of the inlet flow from the end of the manifold. They recommended a recirculation rate of 15%. Trufitt (1975) summarized the advantages for using recirculation:

(1) The main advantage is that a very good distribution performance can be obtained from a flowspreader over a wide operating flow range.

(2) The construction of circular and segmental manifold is simplified if recirculation is used. This is because of the increase in size at the small end and the corresponding increase in manufacturing tolerance.

(3) Recirculation is necessary with rectangular manifolds to prevent unstable flow near the manifold exit.

(4) Recirculation is necessary to sweep the air from manifolds that are oriented to prevent its escape through the tubes.

When recirculation is used, it is important to determine the required rate of recirculation. Figure 3.15 and Figure 3.16 illustrate the effect of recirculation rate on the

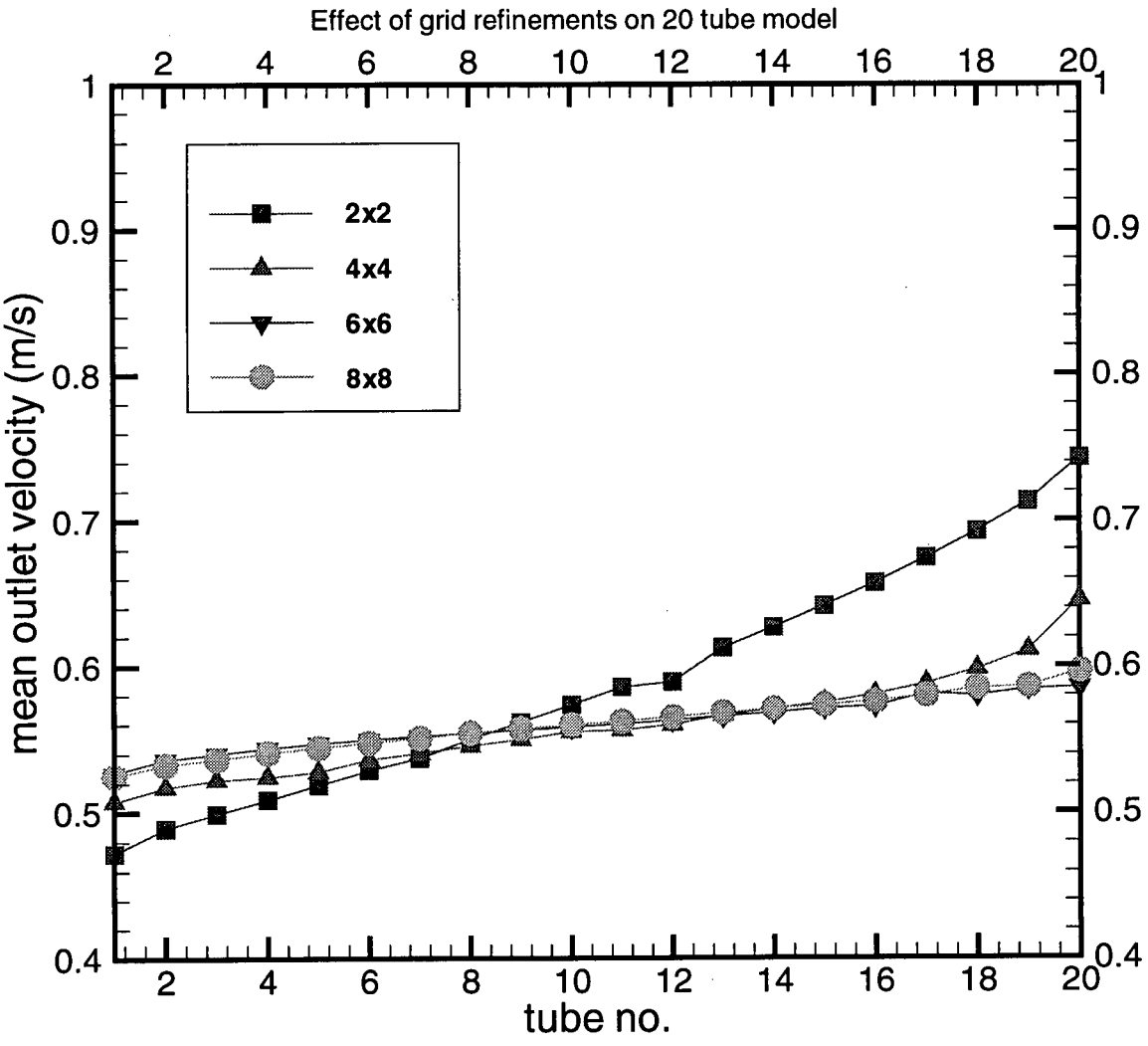

Figure 3.10: Grid independence study of a 20-tube model

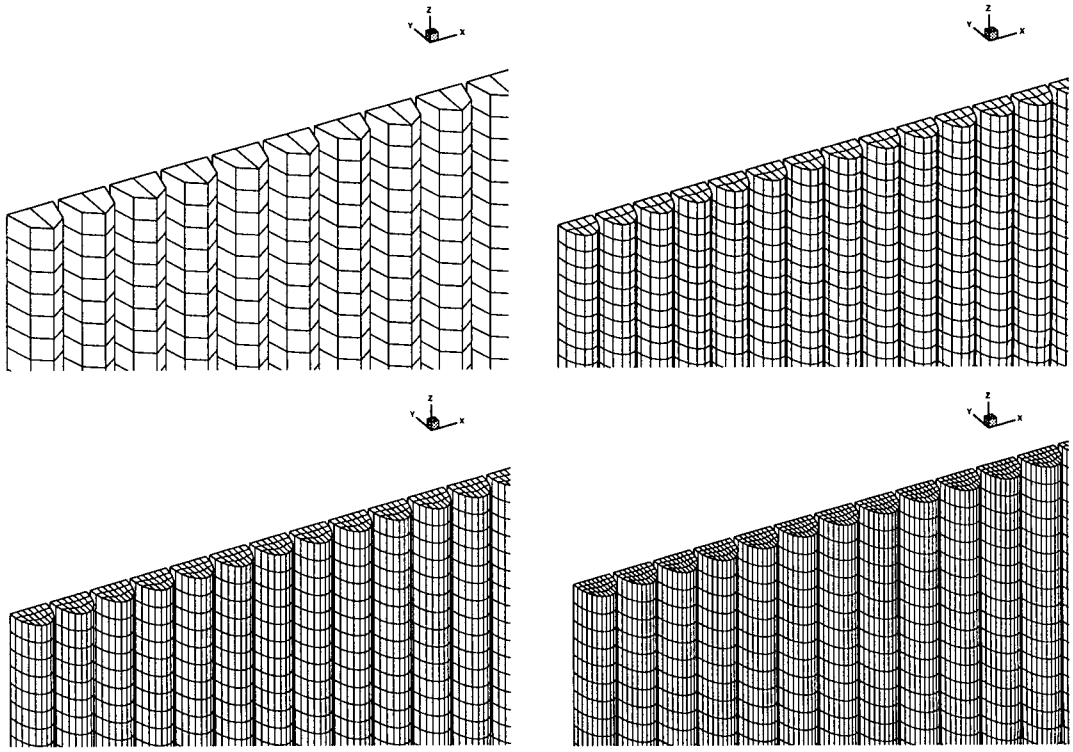

Figure 3.11: Different grid refinement used for 20-tube model study (a) $2 \times 2 \times 30$, (b) $4 \times 4 \times 30$, (c) $8 \times 8 \times 30$, (d) $12 \times 12 \times 30$

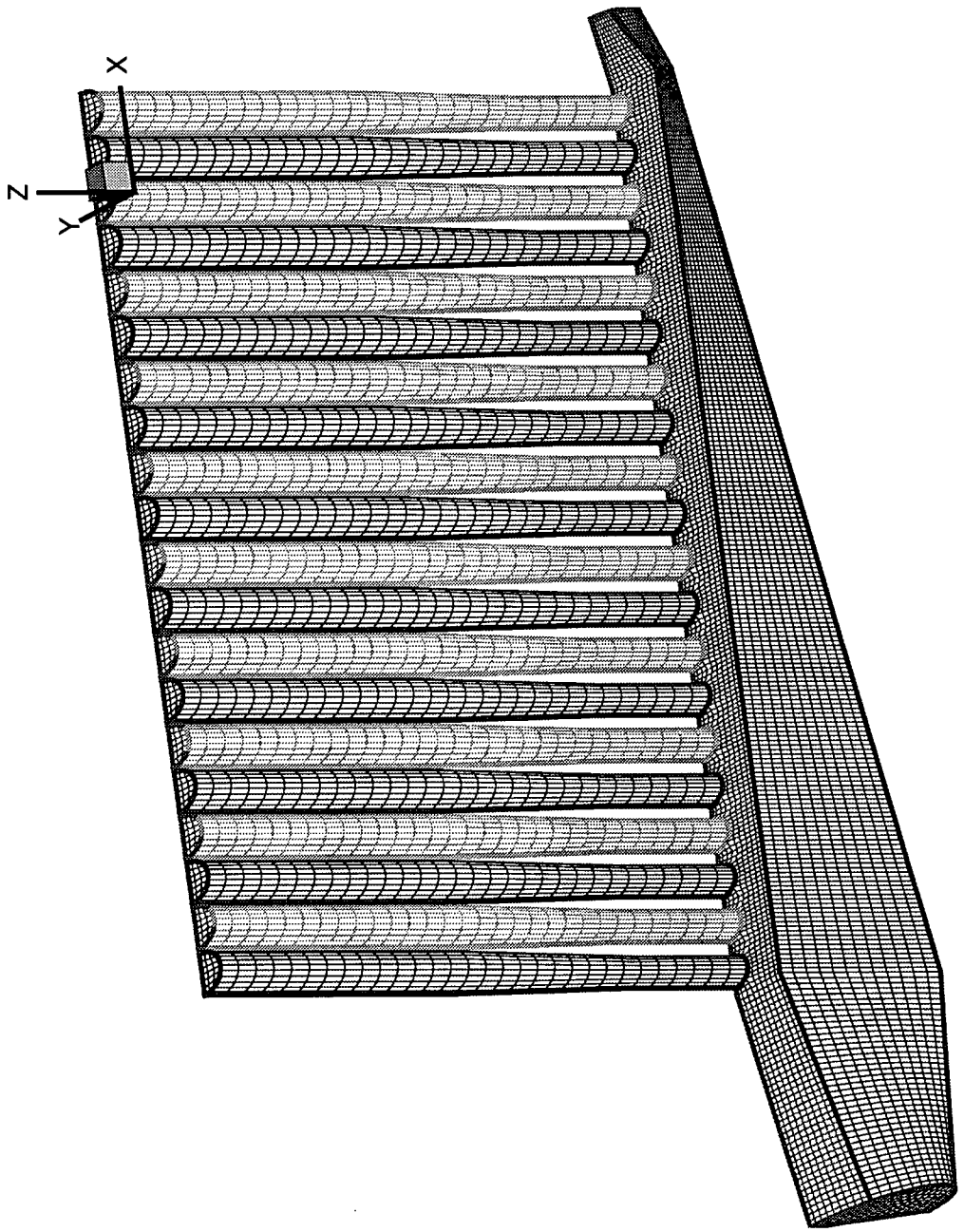

Figure 3.12: Computational grid for the 20-tube model with $6 \times 6 \times 30$ cells for each diffuser tube

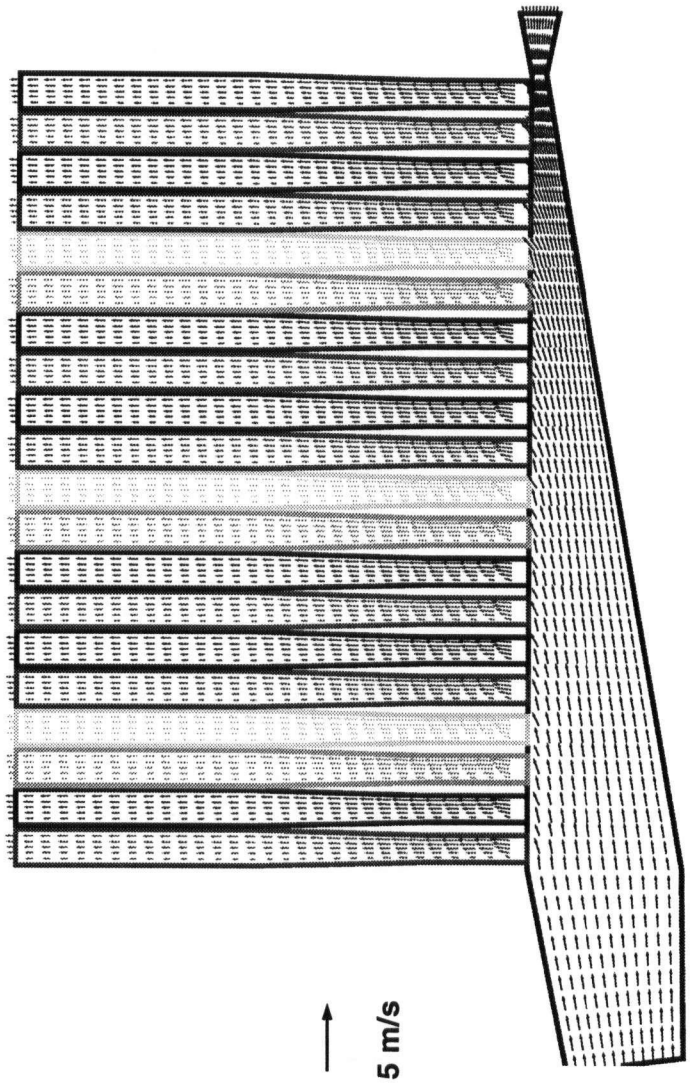

Figure 3.13: Velocity field in the xz-plane

ditribution of flow across the manifold using the 10-tube and 20-tube model respectively. The results show that the recirculation rate has a significant effect on the flow distribution. When the recirculation ratio is 15%, the flow rates of the tubes near the manifold exit drop dramatically compared with other tubes. The zero recirculation rate causes unstable flow in the manifold exit due to highly distorted velocity profiles and the high pressure gradient. The local velocity profile and pressure are shown in Figures 3.17 to 3.20 for 10 and 20-tube model. During this study, the zero recirculation ratio is difficult to converge compared with cases with recirculation.

As mentioned earlier, one main advantage of using recirculation is that good distribution performance can be maintained over a wide operating flow range. In Figure 3.21 and 3.22, the flow rate is increased up to three times the original value, and the uniformity of flow distribution across the manifold is well maintained. These results give solid verification of the advantage of using recirculation.

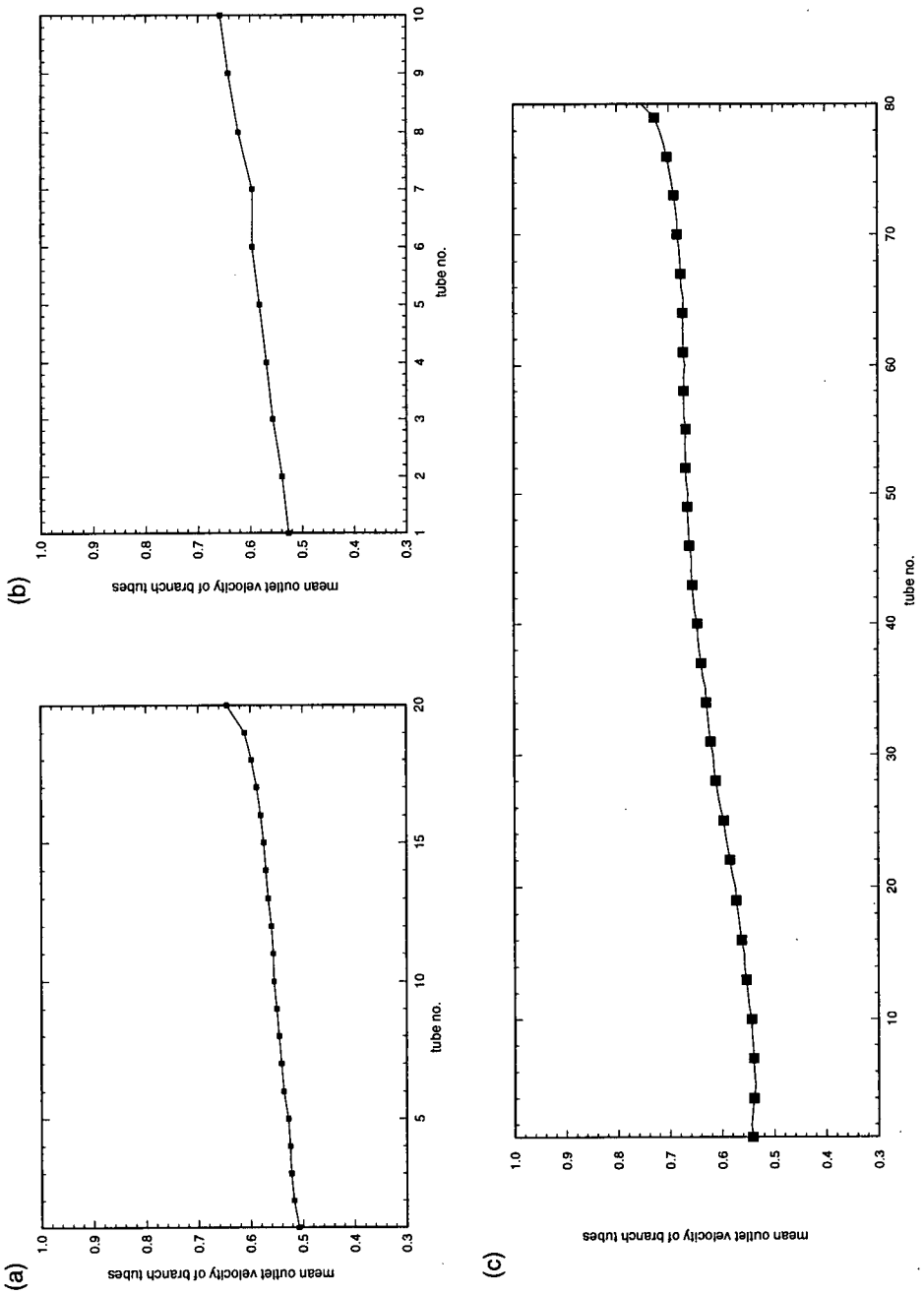

Figure 3.14: The prediction of uniformity of diffuser tube outflow rates using 2×2 cells for the tube cross section (a) 20-tube model (b) 10-tube model (c)real geometry simulation

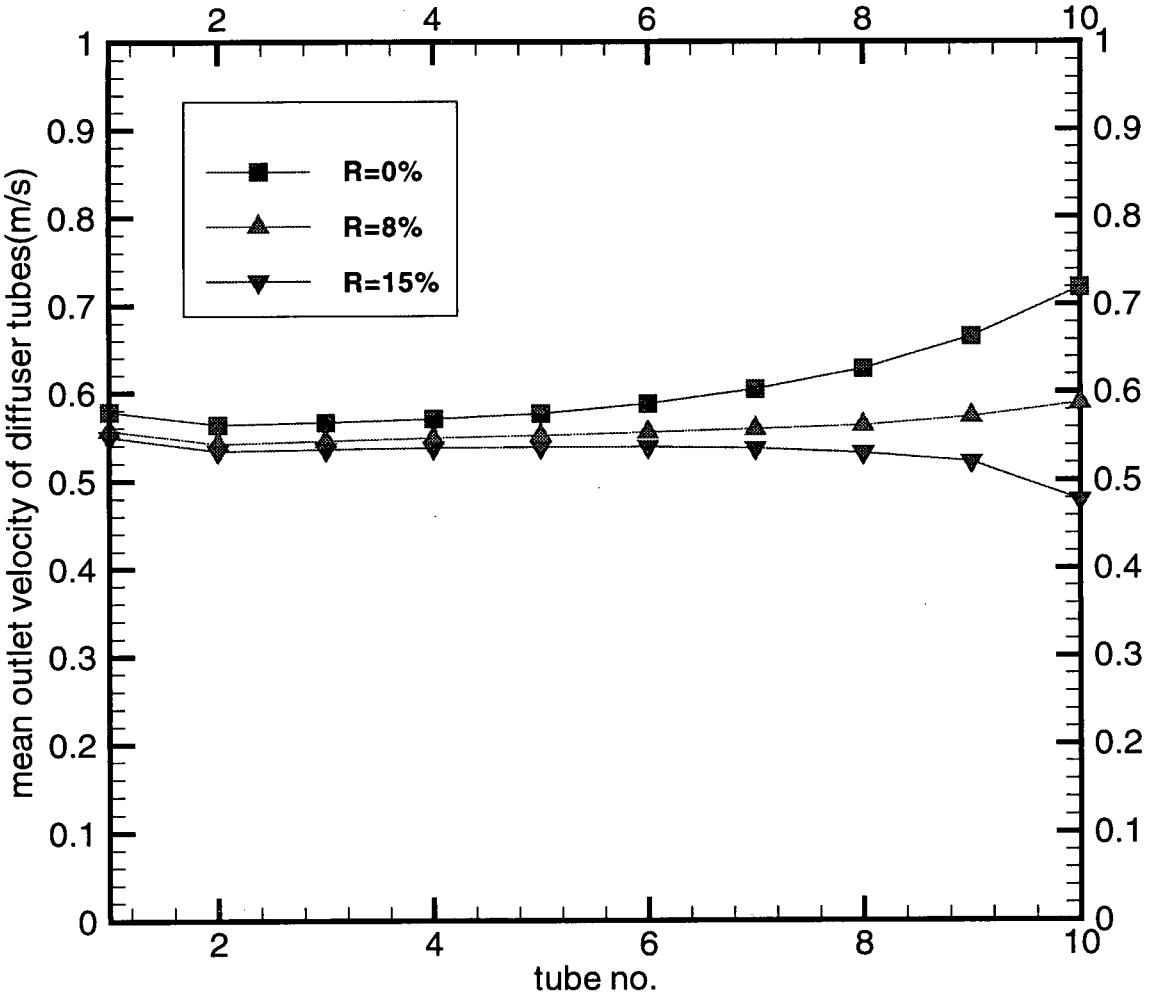

Figure 3.15: Effects of recirculation rate on flow distribution for a 10-tube model

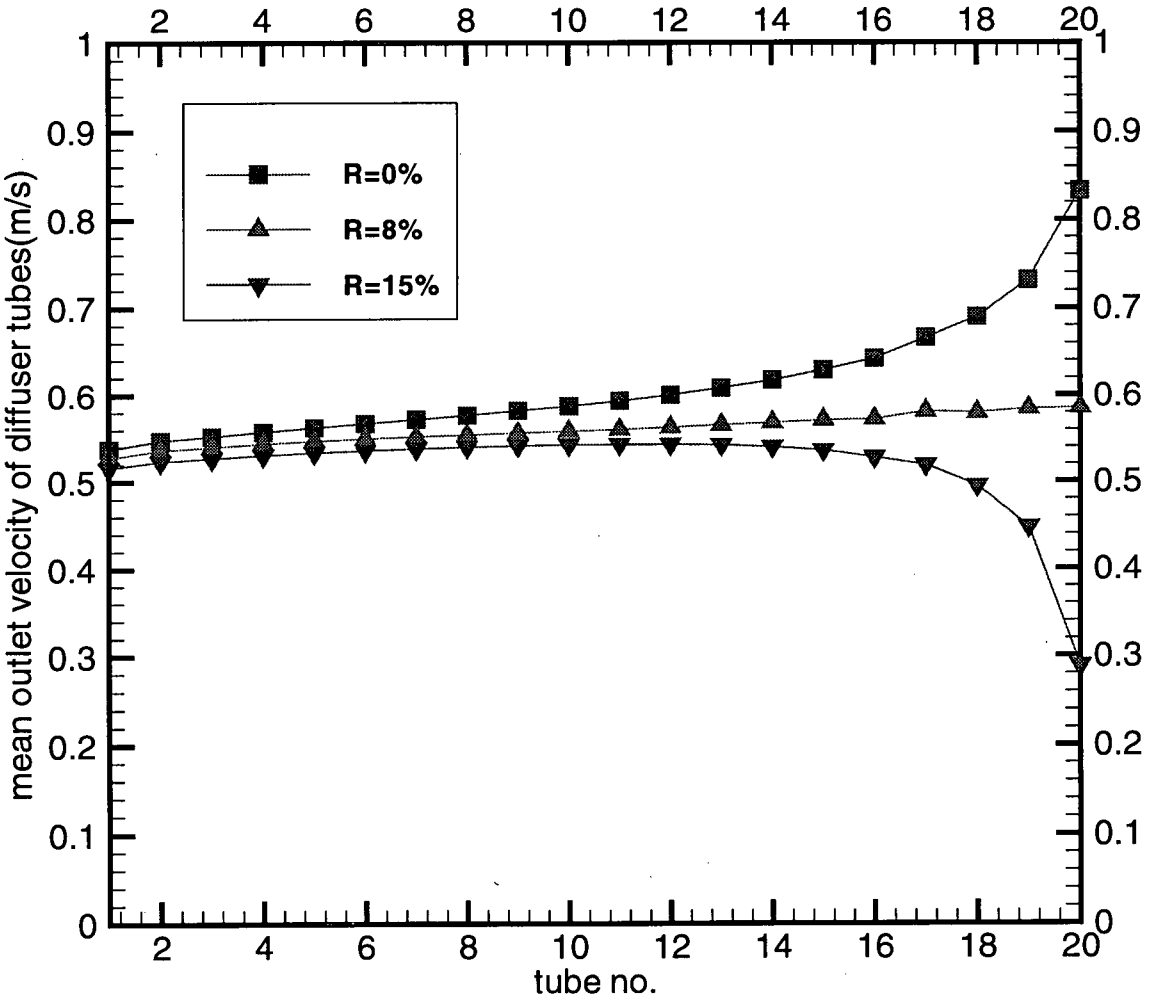

Figure 3.16: Effects of recirculation rate on flow distribution for a 20-tube model

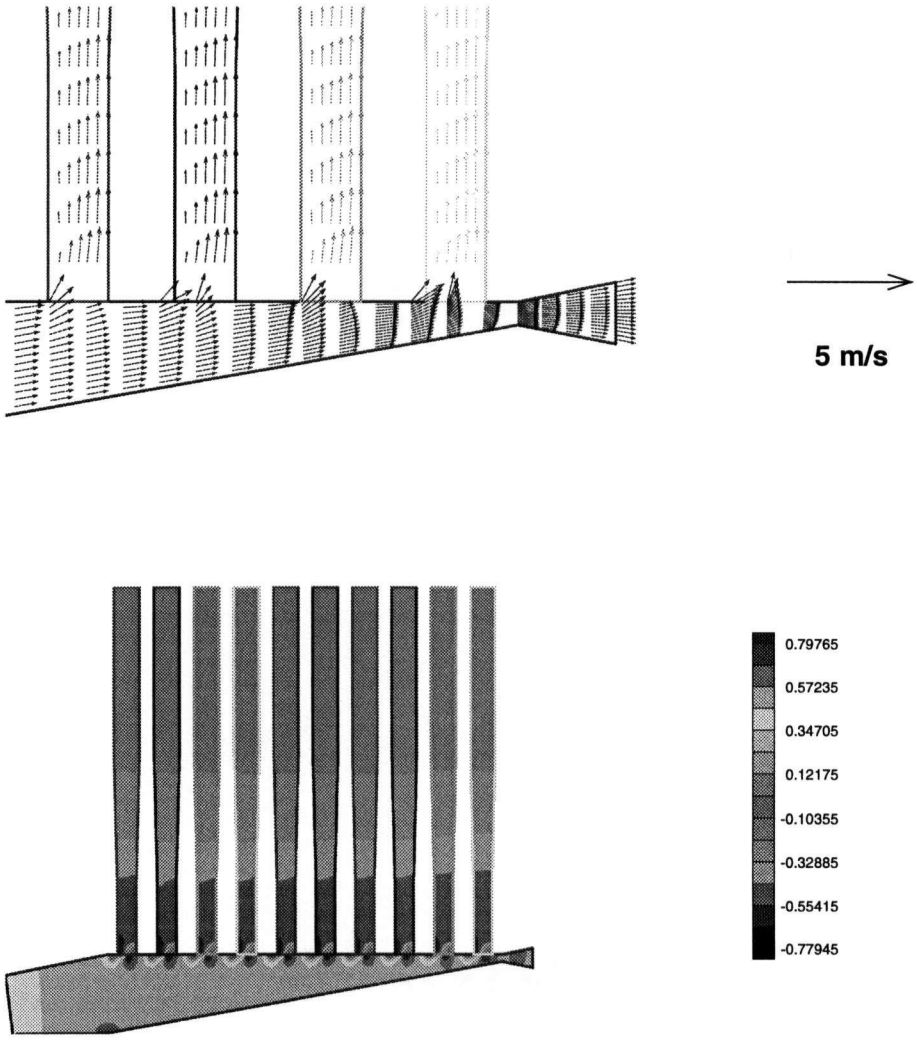

Figure 3.17: Solution at the center plane for a 10-tube model (a) local velocity field (R=8%)(b) pressure distribution (R=8%)

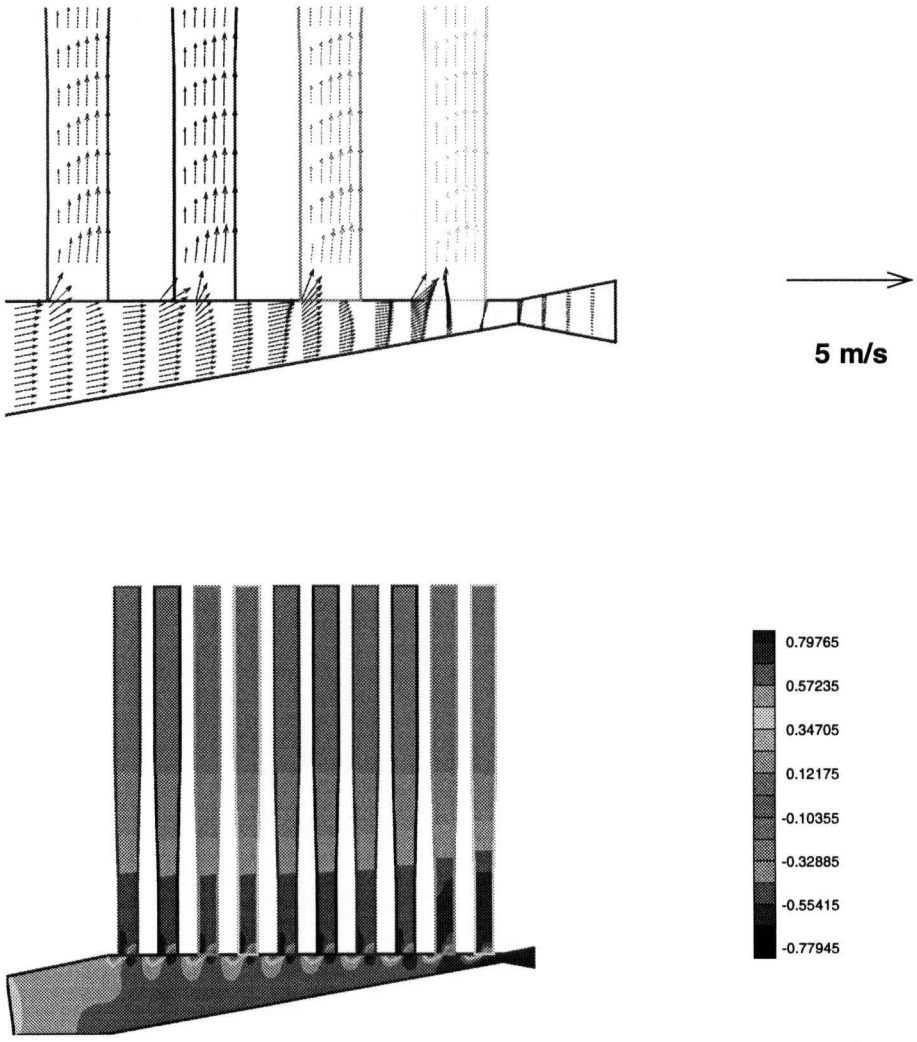

Figure 3.18: Solution at the center plane for a 10-tube model (a) local velocity field (R=0%)(b) pressure distribution (R=0%)

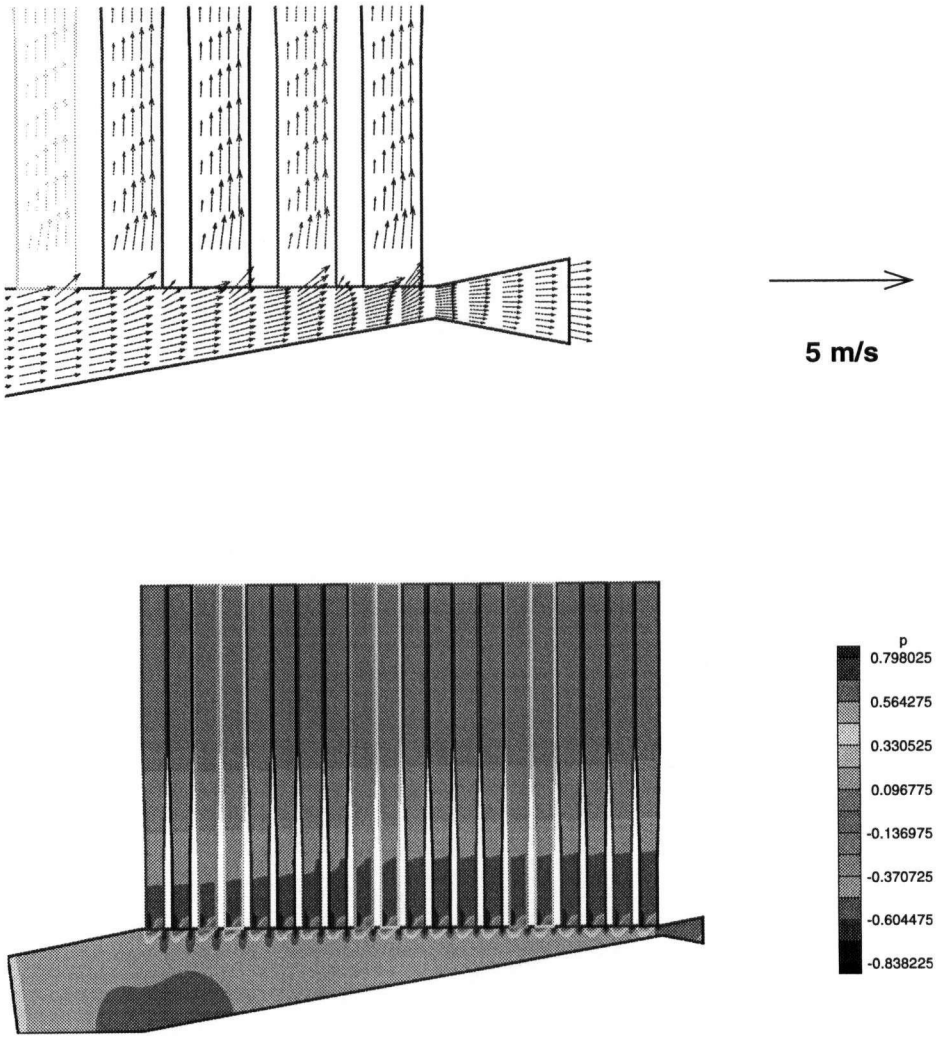

Figure 3.19: Solution at the center plane for a 20-tube model (a) local velocity field (R=8%)(b) pressure distribution (R=8%)

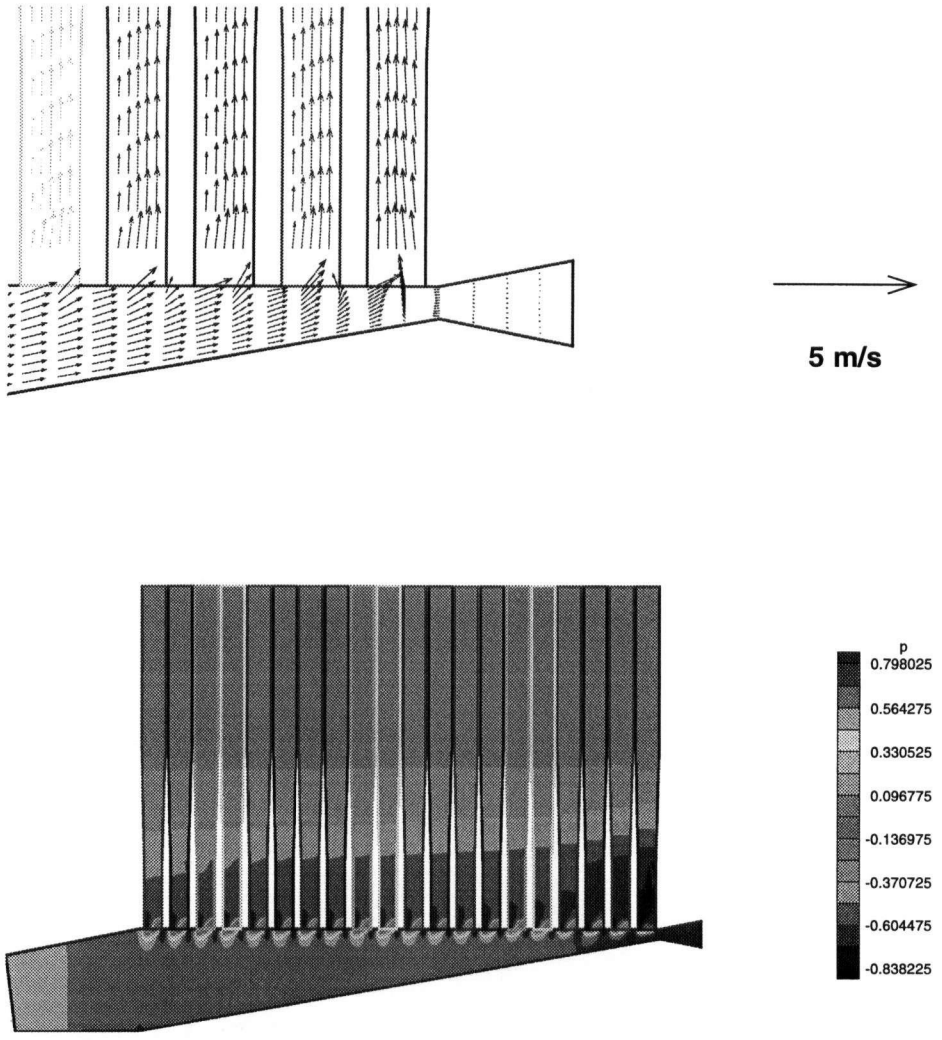

Figure 3.20: Solution at the center plane for a 20-tube model (a) local velocity field (R=0%)(b) pressure distribution (R=0%)

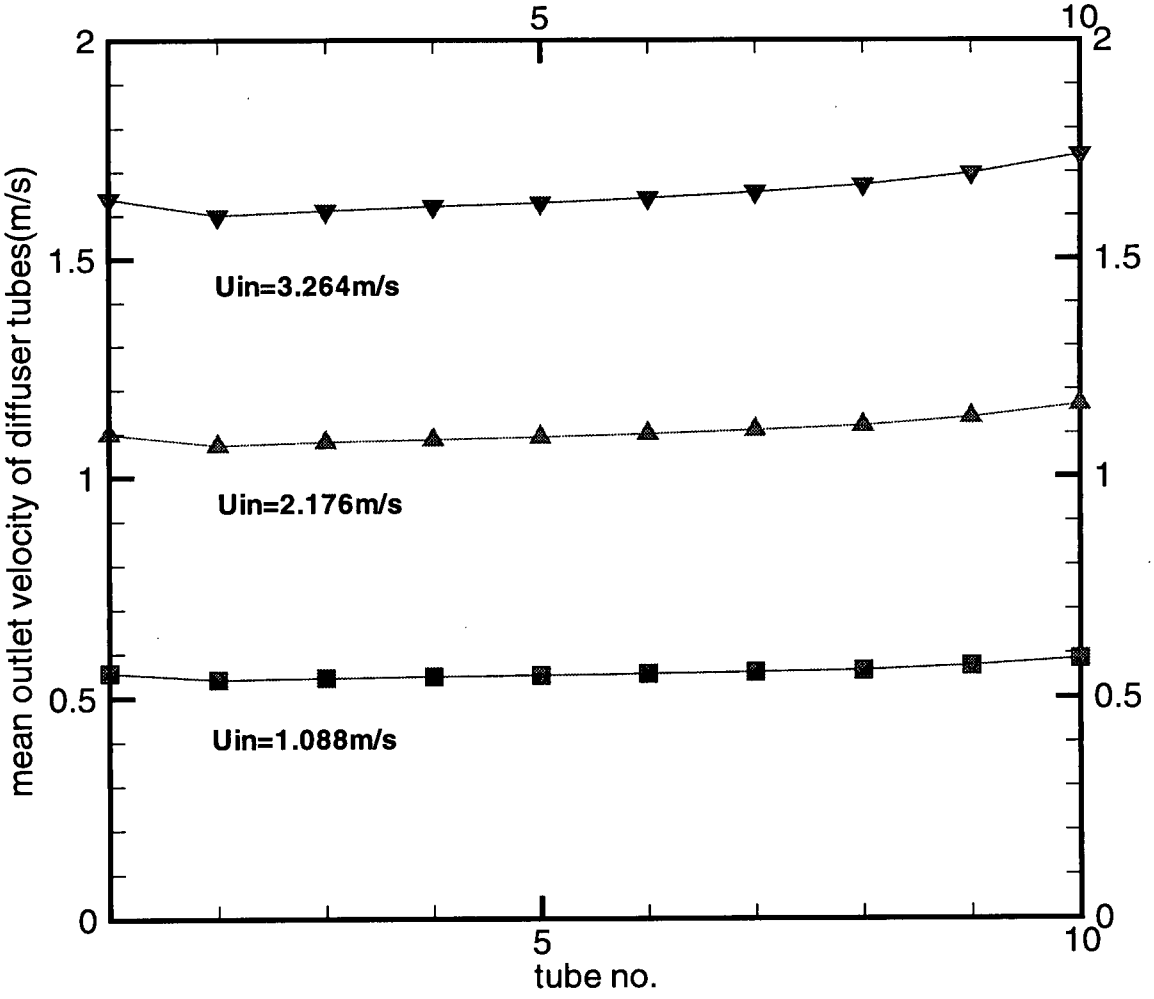

Figure 3.21: Effects of operating flow rate on flow distribution for a 10-tube model with $6 \times 6 \times 30$ grid refinement for each tube and 8% recirculation rate

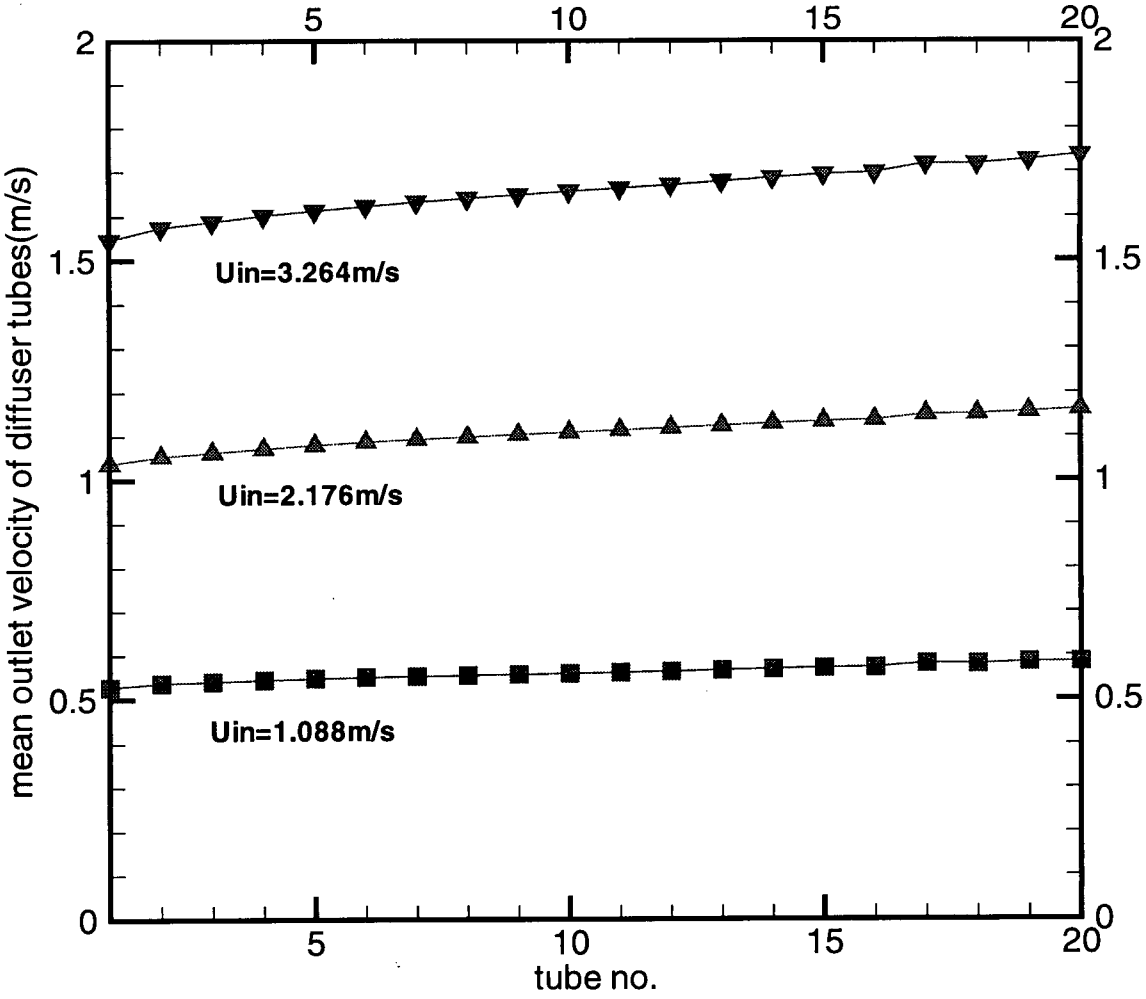

Figure 3.22: Effects of operating flow rate on flow distribution for a 20-tube model with $6 \times 6 \times 30$ grid refinement for each tube and 8% recirculation rate

Chapter 4

Conclusions and Recommendations

4.1 Conclusions

- An existing computational tool has been adapted for the prediction of the flow distribution across manifold type flowspreaders by using a curvilinear grid computational method and elliptic or algebraic grid generation method.

- As a validation of the present computer codes, laminar flow in a simple electronic packaging manifold was computed. This geometry has typical manifold dividing and combining flow characteristics. The prediction of the laminar flow distribution is in good agreement with results reported in the literature showing that the present computational methods can be generalized to deal with manifold type flow domains.

- Calculations using block-structured (multi-block) curvilinear grids are applied to Canfor flowspreader. Grid independence studies were performed for 10 and 20 tube models. The results show that 6×6 cells for the tube cross section are required for the accurate prediction of flow distribution in each tube.

- The real geometry of the Canfor manifold has been simulated together with 10 tube and 20 tube modelling. Due to memory limitations, only coarse grid representation was used for the real geometry simulation. The 10 tube and 20 tube models give results similar to the real geometry simulation do when using same grid refinement. They also predict observations such as the effects of recirculation rate and operating

flow rate on the flow distribution, which are reported in the literature.

- The effects of recirculation rate on the manifold flow distribution are studied using 10 and 20 tube models. It was found the flow rates from the downstream tubes drop dramatically with a 15% recirculation rate, and that the zero recirculation rate causes high pressure and large flow rate from tubes near the end. The results agree with the experimental observation.

- A series of calculations have been performed to study the effect of the operating flow rate on the flow distribution. As reported in the literature, good distribution performance can be maintained over a wide operating flow range by using appropriate value of recirculation.

4.2 Recommendations for Future Work

Some recommendations for future work are suggested:

- The real geometry simulation for the flow diffuser has been limited to coarse grid representation due to computer limitations. An improvement of the computational results can be achieved by using finer grids when larger computer memory is available. In addition, the accuracy of tube models with fewer tubes can be further verified.

- The Canfor manifold has a rectangular cross section, other type of manifold have a segmental cross section (see Figure 4.1) The method preposed in this thesis can be used to model other shapes such as the segmental case.

- The manifold has been studied as an independent flow domain. In the real case, the flow diffuser is connected to other parts of the headbox. The outlet of the diffuser

tubes are the inlet of the contracting parts, as shown in Figure 4.2. The next step must include the contraction part as part of the whole computational domain.

- Grid generation is one of the major tasks in numerical simulation for flows in complex geometries. The grid generation code adapted here, MBEGG, can be used for generating such block-structured, curvilinear grids. However, there are several aspects which require further consideration. In particular, MBEGG has no capability for generating grids with continuous grid slopes across the interfaces between domains. Smooth grid interface could perhaps be obtained by iteratively adjusting the source terms near the interface.

Figure 4.1: Manifold with segmental cross section

Figure 4.2: Manifold with the contracting par

Appendix A

A Computational Method Using Curvilinear Grids - CMGFD

The CMGFD code was developed by He (1995) based on a previous CFD code, MGFD, developed by Nowak (1992) in the research group at UBC supervised by M.Salcudean and I. Gartshore. The MGFD code is a comprehensive 3D numerical code with multigrid and domain segmentation techniques. However, its application is limited to rectangular type geometries since it is based on the Cartesian coordinate system. The CMGFD code uses block-structured curvilinear grids. All the techniques used in the MGFD code, such as the multigrid method and domain segmentation feature, are generalized into the CMGFD code.

The CMGFD code involves several numerical techniques. These techniques are implemented in the code in four steps as reported by He (1995).

In the first step, the calculation of laminar flow in complex geometry using general curvilinear grids is investigated. This step is necessary to develop an efficient, curvilinear coordinate-based finite-volume method while avoiding the additional complexity of turbulence modeling and domain segmentation treatments. Finite-volume methods in conjunction with curvilinear grids have become popular in recent years for flow simulation in complex geometry. However, problems still exist in terms of the accuracy and efficiency of such computations. In the present study, a finite volume method using general curvilinear grids is proposed to overcome some of these difficulties. The coordinate invariant conservation equations and the physical geometric quantities of the control cells are used

directly to formulate the numerical scheme without reference to the commonly-used covariant and contravariant vectors. The definitions of the physical geometrical quantities and the tangential velocity unknowns are introduced. A new difference scheme for the non-orthogonal diffusion and pressure terms is proposed. This scheme contributes to the main diagonal terms in the resulting coefficient matrix and allows an implicit treatment of the non-orthogonal quantities without increasing the number of computational molecules. A coupled equation solver is used in place of the commonly-used pressure-correction equation associated with grid non-orthogonality. The developed method is implemented in the CMGFD code. Several two- and three-dimensional laminar flows are computed and compared with other numerical, experimental and analytical results to validate the solution method and code (see He (1995)).

In the second step, the method developed in the first step is generalized to turbulent flows. It is well known that turbulent flows are more difficult to handle. This step is intended to increase our knowledge in dealing with turbulent flows in the environment of general curvilinear grids and achieve an efficient numerical method for turbulent flows. The mathematical model adopted for the present study is introduced. The $k-\epsilon$ two-equation model together with the 'wall function' is used to simulate turbulent flows. The discretization of the $k-\epsilon$ equations and the formulation of the 'wall function' are presented. The treatment of the source terms in the $k-\epsilon$ equations is discussed in detail. The performance of the method is investigated through several three-dimensional turbulent flows to validate the method as well as the CMGFD code in He (1995).

The third step is concentrated on the development of an efficient multigrid method for flow simulation in general curvilinear grids. The multigrid method is an efficient solution procedure which exhibits convergence rates insensitive to grid refinement. It has been widely used in the field of computational fluid dynamics. However, there have been

relatively few studies carried out using general curvilinear grids. There are additional difficulties for multigrid acceleration in curvilinear coordinate systems which require careful consideration.

In the CMGFD code, a multigrid method for calculating laminar and turbulent flows using general curvilinear grids is developed. First, the multigrid calculation of laminar flows is studied with emphasis on the influence of complex flow boundaries. It is found that the discrete governing equations on different grid levels can become inconsistent in some curvilinear grids due to complex flow boundaries, thus reducing the efficiency of the multigrid algorithm. A novel treatment is proposed to solve this problem. Secondly, the difficulties associated with the multigrid acceleration of turbulent flows are discussed and several techniques which help the performance of the multigrid method are introduced. Particularly, it is found that the formulation of the coarse-grid defect equation using the 'wall function' can cause inconsistency of the governing equations between fine and coarse grids. This problem is discussed in detail and a novel approach is proposed to allow the successful implementation of the multigrid method for turbulent flows.

In the last step, the method developed in the three previous steps is generalized to non-structured curvilinear grids by using a domain segmentation technique. This technique divides the domain of interest into different sub-domains. Solutions are obtained by iteratively applying the solver described in the previous steps to each sub-domain. The implementation of the domain segmentation strategy in the method using general curvilinear grids is studied. Particular attention is given to the communication between neighbouring sub-domains. The performance of the multi-block method is investigated through several computational examples in He (1995).

The methods described above have been implemented in the CMGFD code. With the above developments the code can be used to deal with arbitrary complex geometry

if proper block-structured curvilinear grids are generated. However, generating appropriate grids is often a difficult task. The existing difficulty in generating appropriate grids is one of the reasons that few numerical studies are carried out over complex three dimensional domains. An elliptic grid generation code, MBEGG, is developed to support the application of the CMGFD code. It can be used to generate multi-block curvilinear grids for various complex flows. An elliptic grid generation method is used in the code, which solves three nonlinear elliptic grid generation equations. The source terms in the equations are problem-dependent functions and can be used to control the grid characteristics, such as orthogonality and grid stretching. Methods to achieve certain grid quantities, such as skewness, through the control functions are implemented in the code. The multigrid method is an ideal solver for the elliptic grid generation equations due to the fully elliptic nature of the equations. In the present study, a multigrid method is developed to solve these equations. A domain segmentation technique is adopted in the code to generate block-structured curvilinear grids. Block-structured curvilinear grids are generated for flows over manifold type flow spreaders using the code.

Appendix B

Governing Equations

In this section, the governing equations and turbulence model used in the present study are described. The full, Reynolds-averaged Navier-Stokes equations together with the standard $k-\epsilon$ equations are solved for turbulent flows. Using the eddy viscosity concept and the closure of the $k-\epsilon$ two-equation model of Launder and Spalding (1974), the averaged governing equations for steady, incompressible flows can be written in the following coordinate-free form:

$$\varrho \mathbf{u} \cdot \nabla \mathbf{u} - \nabla \cdot (\mu_{eff} \nabla \mathbf{u}) = - \nabla p, \tag{B.1}$$

$$\nabla \mathbf{u} = 0, \tag{B.2}$$

$$\nabla \cdot (\varrho \mathbf{u} k - \frac{\mu_t}{\sigma_k} \nabla k) = G - \varrho \epsilon, \tag{B.3}$$

$$\nabla \cdot (\varrho \mathbf{u} \epsilon - \frac{\mu_t}{\sigma_\epsilon} \nabla \epsilon) = C_1 \frac{\epsilon}{k} G - \varrho C_2 \frac{\epsilon^2}{k}, \tag{B.4}$$

where k is the turbulence kinetic energy, ϵ is the turbulence energy disspation rate, ϱ is the flow density, G is the turbulence energy generation rate, C_1, C_2, σ_k and σ_ϵ are empirical constants which, following Launder and Spalding (1974), are taken as

$$C_1 = 1.44, \quad C_2 = 1.92, \quad \sigma_k = 1.0, \quad \sigma_\epsilon = 1.3, \quad C_\mu = 0.09.$$

Equations (3.1) and (3.2) represent the momentum and mass conservations, respectively, for steady, incompressible flows, and are the well-known Reynolds-averaged Navier-Stokes equations. Equations (3.3) and (3.4) are the transport equations for turbulence kinetic

energy and its dissipation rate respectively. In these equations, $\mathbf{u}$ is the mean velocity vector which is time-averaged from the instantaneous velocity, $\bigtriangledown\mathbf{u}$ is a tensor, and μ_{eff} is the effective viscosity which is given by:

$$\mu_{eff} = \mu_t + \mu_l,$$

where μ_l and μ_t are the laminar and the turbulent viscosities respectively. The turbulent viscosity is evaluated from the relation

$$\mu_t = \varrho C_\mu k^2/\epsilon, \tag{B.5}$$

where C_μ was found empirically to be approximately constant at high Reynolds numbers.

Appendix C

Grid Generation for Manifolds with a Circular Cross Section

C.1 Problem Description

The circular cross section manifold under consideration has a large plenum and four diffuser tubes, as shown in Figure C.1.

The inlet diameter of the large plenum is $1m$ and the outlet diameter is $0.225m$. Each diffuser tube is $2m$ long with an inlet diameter of $0.2m$.

C.2 Computational Grid

The computational domain is segmented into a main flow subdomain and four diffuser flow subdomains. In order to obtain a continuous grid between the main flow domain and the diffuser tubes, rectangular grids are used for the diffuser tubes instead of cylindrical grids which have a singular line at the center. The two different types of grids are shown in Figure C.2.

The direct grid generation for the main flow subdomain is difficult. The method adopted here is to generate two dimensional grid first, then map the grid into a three dimension grid. (Figure C.3)

The grid generation method developed by He (1995) can be modified to generate the grid for a circle inside a rectangle as shown in Figure C.4.

Grids for the present 2D geometry cannot be generated by the method developed by He (1995). A new subroutine called multicircle was developed here to generate the grid.

In the multicircle code, a method similar to the 3D multi-block grid generation method is used to generate grids for 2D geometries. In this method, the entire complex geometry is divided into different parts, grids are generated in each part and then patched together.

The 2D grid and the 3D surface grid after mapping are shown in Figure C.5. The complete computational grid for the manifold is shown in Figure C.6.

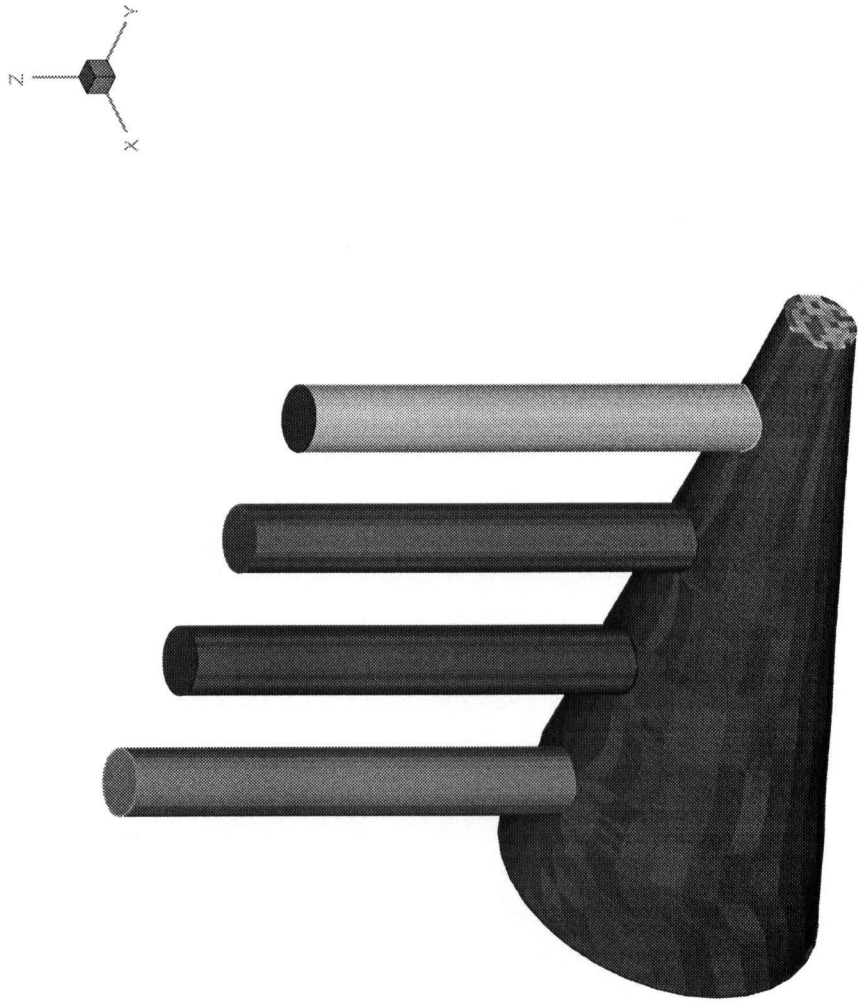

Figure C.1: Illustration of the circular cross section manifold

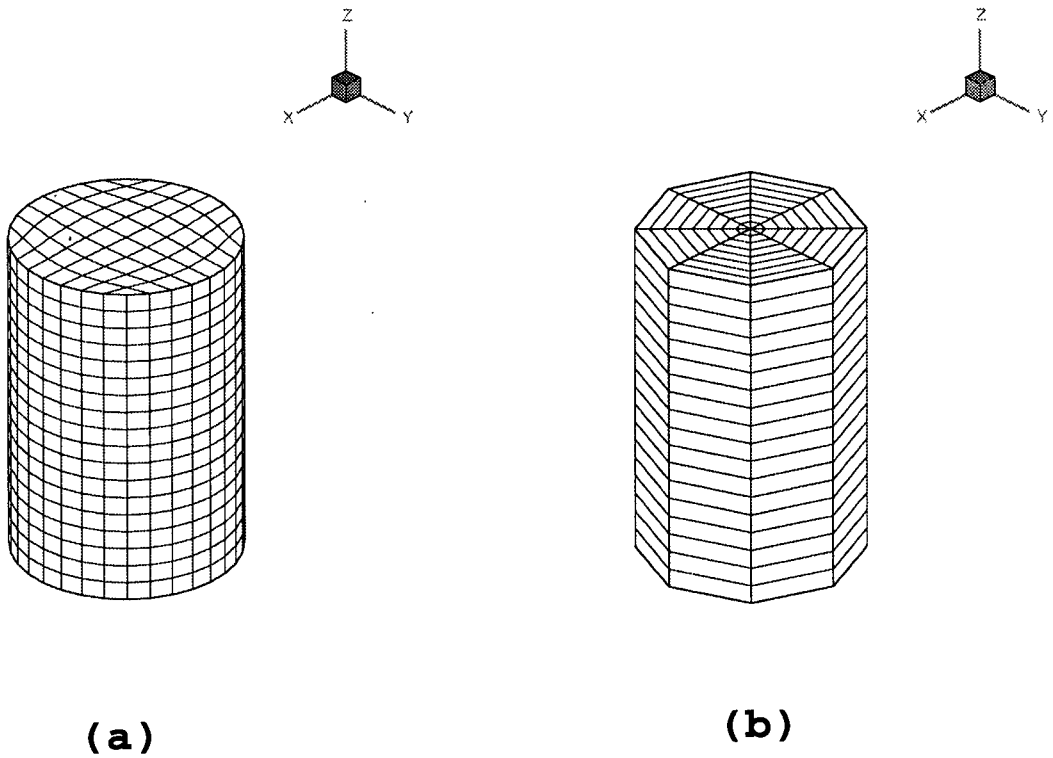

Figure C.2: Illustration of the two different types of grids for the diffuser tube. (a) Rectangular (b) Circular

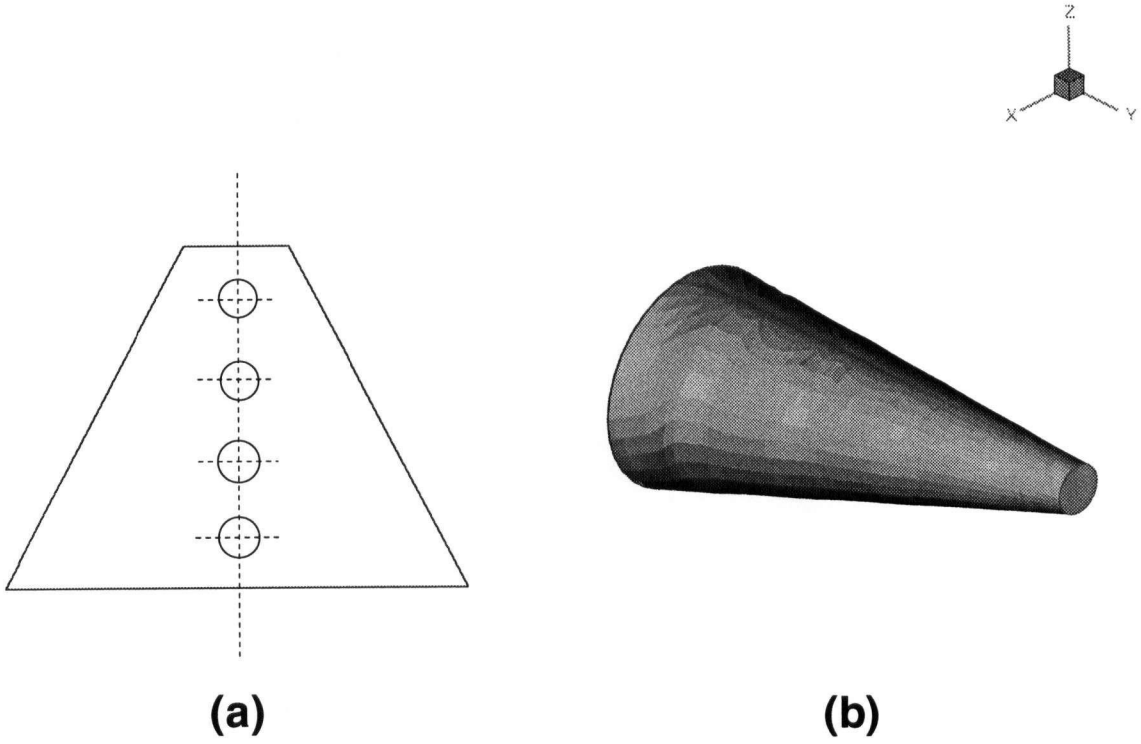

Figure C.3: Illustration of the geometry mapping from 2D to 3D

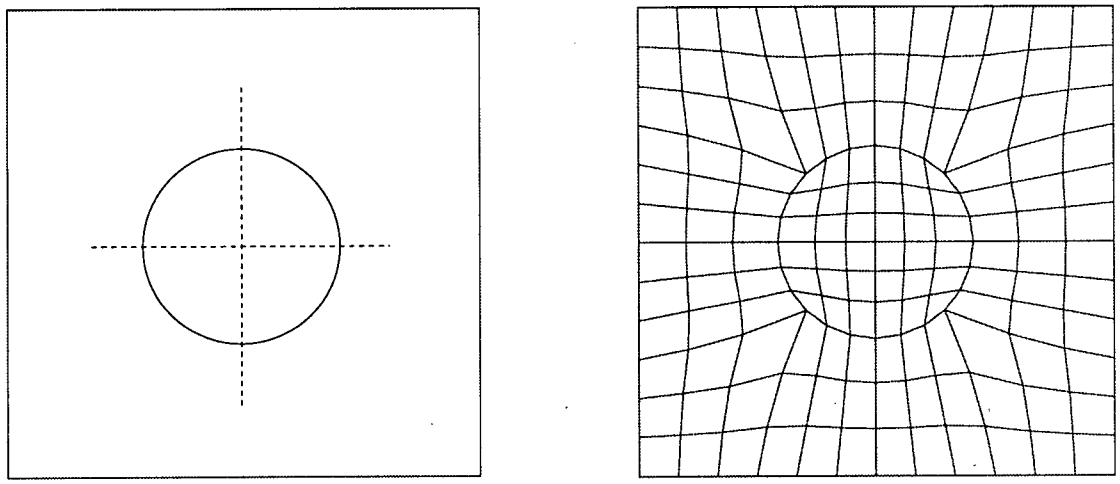

Figure C.4: Grid generation for a circle inside a rectangular

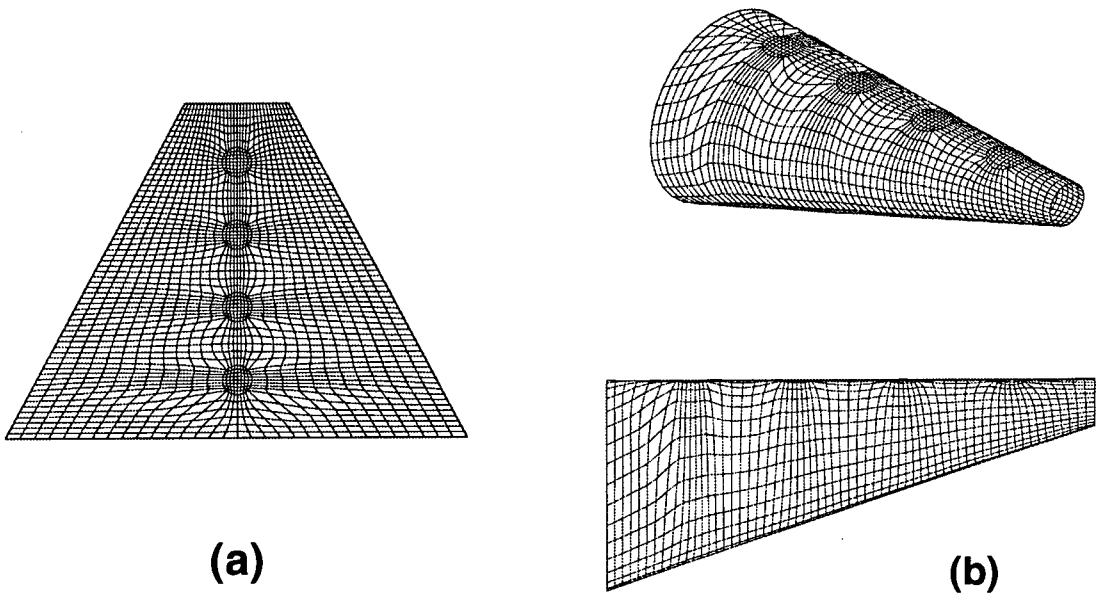

Figure C.5: Illustration of the 2D and 3D surface grid for the circular cross section manifold

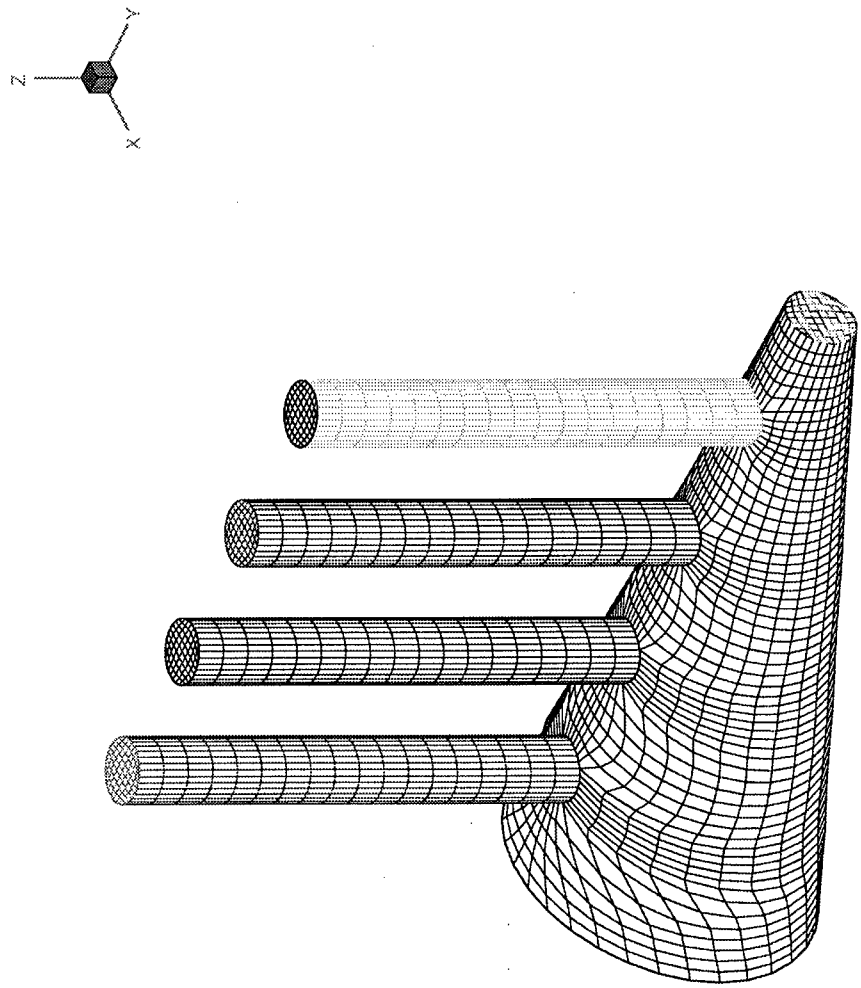

Figure C.6: Illustration of the complete manifold computational grid

Bibliography

[1] W. Baines, C.I.H. Nicholl, R.C. Cook and J. Mardon, 1956, "The taper flow headbox (a new design concept)", Pulp and Paper Magazine of Canada, Vol. 57, No. 11, pp. 139-148.

[2] M.E. Braaten and W. Shyy, 1986, "Comparison of iterative and direct solution methods for viscous flow calculations in body-fitted coordinates", Int. J. Num. Meth. in Fluids, Vol. 6, pp. 325-349.

[3] M. E. Braaten and S. V. Patankar, 1989, "A block-corrected subdomain solution procedure for recirculating flow calculation", Num. Heat Transfer, Part B, Vol. 15, pp. 1-20.

[4] A. Brandt, 1981, *Guide to Multigrid Development, Lecture Notes in Mathematics*, 960, Springer-Verlag, New York.

[5] L. S. Caretto, R. M. Curr, and D. B. Spalding, 1972 "Two numerical methods for three-dimensional boundary layers", Comp. Meth. Appl. Mech. Eng., Vol.1, pp. 39-57.

[6] S.H. Choi, S. Shin and Y.I. Cho, "The effect of area ratio on the flow distribution in liquid cooling module manifolds for electronic packaging", 1993, Int. Comm. Heat Mass Transfer, Vol. 20, pp. 221-234.

[7] L. Davidson and P. Hedberg, 1989, "Mathematical derivation of a finite volume formulation for laminar flow in complex geometries", Int. J. Numer. Methods Fluids, Vol.9, pp.531-540.

[8] I. Demirdzic, A. D. Gosman, R. I. Issa and M. Peric, 1987, "A calculation procedure for turbulent flow in complex geometries", Comp. & Fluids, Vol. 15, pp. 251-273.

[9] I. Demirdzic, Z. Lilek and M. Peric, 1992, "Fluid flow and heat transfer test problems for non-orthogonal grids: bench-mark solutions", Int. J. Numer. Methods in Fluids, Vol. 15, pp. 329-354.

[10] Q. V. Dihn, R. Glowinsi, and J. Periaux, *Solving Elliptic Problems by Domain Decomposition Methods with Applications*, in G. Birkhoff and A. Schoenstadt (eds.), Elliptic Problem Solvers II, Academic Press, New York, 1984.

[11] M.M. Eanyet, M.M. Gibson, A.M.K.P. Taylor and M. Yianneskis, 1982, "Laser-doppler measurements of laminar and turbulent flow in a pipe bend", Int. J. Heat and Fluid Flow, Vol. 3 pp. 213-219.

[12] M.L. Enger and M.I. Levy, 1929 "Pressure in manifold pipes", J. Am. Water Works Assoc. Vol. 21 pp. 659-667

[13] M. Faghri, E.M. Sparrow, and S.T. Prata, 1984, "Finite difference solutions of convection diffusion problems in irregular domains using nonorthogonal coordinate transformation', Numer. Heat Transfer, Vol. 7, pp. 183-209.

[14] H. Fu, A. P. Watkins, M.J. Tindal and M. Yianneskis," Computation of three-dimensional turbulent flows in a pipe junction with reference to engine inlet manifold", Proceedings of the Institution of Mechnical Engineers. Journal of Mechnical Engineering Science, 1992, Vol. 206, pp. 285-296.

[15] P. F. Galpin, J. P. Van Doormaal, and G. D. Raithby, 1985, "Solution of the incompressible mass and momentum equations by application of a coupled line solver", Int. J. Numer, Methods Fluids, Vol. 15, pp. 615-625.

[16] P. He, "Numerical prediction of film cooling of turbine blades using multiblock curvilinear grids", Ph.D. Thesis (1995), Dept. of Mech. Eng., University of British Columbia.

[17] P. He and M. Salcudean, "A numerical method for 3D viscous incompressible flows using non-orthogonal grids", J. of Numer. Method in Fluids, Vol. 18, pp. 449-469.

[18] P. He, M. Salcudean and I.S. Gartshore, 1994, "Multigrid calculation of laminar and turbulent flows using general curvilinear grids", Proc. of CFD94 of Canada, Toronto.

[19] P. He, M. Salcudean and I.S. Gartshore, " Computations of film cooling for the leading edge region of a turbine blade model", Preprint, (1994).

[20] P. He, M. Salcudean and I. S. Gartshore, 1993, "A nonlinear multigrid algorithm for grid generation", Technical Report, The Department of Mechanical Engineering, UBC.

[21] P. He, *CMGFD: A 3D Curvilinear Coordinate-Based Multi-Block Multigrid CFD Code*, Technique, CFD group, Dept. of Mech. Eng., The University of British Colubia.

[22] M. Hinatsu and J. H. Ferziger, 1991, "Numerical computation of unsteady incompressible flow in complex geometry using a composite multigrid technique", Int. J. Numer. Methods Fluids, Vol. 13, pp. 971-997.

[23] G.L. Jones and R.J. Ginnow, 1988, "Modelling headbox performance with computational fluid mechanics", TAPPI Engineering Conference, Chicago, Illinois, pp. 15-20.

[24] D. S. Joshi and S. P. Vanka, 1991, "Multigrid calculation procedure for internal flows in complex geometries", Numer. Heat Transfer, B, Vol. 20, pp. 61-80.

[25] K.C. Karki and S.V. Patankar, 1988, "Calculation procedure for viscous incompressible flows in complex geometries", Numer. Heat Transfer, Vol. 14, pp. 295-307.

[26] A. Klein, 1981, "REVIEW: Turbulent developing pipe flow", J. Fluids Eng., Vol. 103, pp. 242-249.

[27] B. E. Launder and D. B. Spalding, 1974, "The numerical computation of turbulent flows", Comp. Meth. Appl. Mech. Eng., Vol. 3, pp. 269-275.

[28] D. Lee and J.J. Chiu, 1992, "Covariant velocity-based calculation procedure with nonstaggered grids for computation of pulsatile flows", Numer. Heat Transfer, Part B, Vol. 21, pp. 269-286.

[29] M. A. Leschziner and K. P. Dimitriadis, 1989, "Computation of three-dimensional turbulent flow in non-orthogonal junctions by a branch-coupling method", Comp. Fluids, Vol. 17, pp. 371-396.

[30] J.H. Leylek and R.D. Zerkle, 1993, "Discrete-jet film cooling: A comparison of computational results with experiments", ASME 93-GT-207.

[31] C.R.Maliska and G.D.Raithby, 1984, "A method for computing three dimensional flows using non-orthogonal boundary-fitted coordinates", Int. J. Numer. Methods Fluids, Vol. 4, pp. 518-537.

[32] J. Marton and C.I.H. Nicoll, 1960, U.S. Patent 2.929.949

[33] J. Marton, R.E. Monashan and E.S. Brown, "The design of paper machine headboxes for optimum wire flow and formation", APPITA Vol. 18, No. 5, pp. 201-219

[34] J. Marton, D.W. Manson, J.E. Wilder, R.E. Monashan, A.D. Trufitt and E.S. Brown, 1963, "The design of manifold systems for paper machine headboxes. Part 2: Taper flow manifolds", TAPPI, Vol. 46, No. 3, pp. 172-187.

[35] J. Marton, R.E. Monashan and E.S. Brown, "Experimental Investigation of Manifold Systems for Paper Machine Headboxes", Pulp and Paper Magazine of Canada, 1965, Vol. 66, No. 9, pp. 459-474.

[36] J. Marton, E.G. Hauptman, R.E. Monashan and E.S. Brown, " The Extant State of the Manifold Problem", Pulp and Paper Magazine of Canada, 1971, Vol. 72, No. 11, pp. 76-81.

[37] M.C. Melaaen, 1992, "Calculation of Fluid Flows with Staggered and Nonstaggered Curvilinear Nonorthogonal Grids- Theory", Numer. Heat Transfer, Part A, Vol. 21, pp. 1-20.

[38] P. Nowak, 1992, "A multigrid and multi-block method", Technique Report, The University of British Columbia.

[39] C. W. Oosterlee and P. Wesseling, 1992, "A multigrid method for an invariant formulation of the incompressible navier-stokes equations in general co-ordinates", Comm. Applied Nume. Methods, Vol. 8, pp. 721-734.

[40] S.V. Patankar, *Numerical Heat Transfer and Fluid Flow*, Hemisphere, Washington, D.C., 1980.

[41] C.Y. Perng and R.L. Street, 1991, "A coupled multigrid-domain-splitting technique for simulating incompressible flows in geometrically complex domains", Int. J. Numer. Methods Fluids, Vol. 13, pp. 269-286.

[42] M. Perić, 1990, "Analysis of pressure-velocity coupling on nonorthogonal grids", Numer. Heat Transfer, Part B, Vol. 17, pp. 63-82.

[43] D. Rayner, 1991, "Multigrid flow solutions in complex two-dimensional geometries", Int. J. Numer. Methods in Fluids, Vol. 13, pp. 507-518.

[44] J.W. Richman and R.S. Azad, 1973 "Developing turbulent flow in smooth pipes", Apl. Sci. Res., Vol. 28, pp. 419-441.

[45] W. Rodi, S. Majumdar, and B. Schonung, 1989, "Finite volume methods for two-dimensional incompressible flows with complex boundaries", Comp. Meth. in Appl. Mech. and Eng., Vol. 75, pp. 369-392.

[46] M. Rosenfeld, D. Kwak and M. Vinokur, 1988, "A solution method for the unsteady incompressible Navier-Stokes equations in generalized coordinate systems", AIAA Paper AIAA-88-0718.

[47] P. A. Rubini, H. A. Becker and E. W. Grandmaison, A. Pollard, A. Sobiesiak and C. Thurgood, 1992, "Multigrid acceleration of three-dimensional, turbulent, variable-density flows", Numer. Heat Transfer, Part B, Vol. 22, pp. 163-177.

[48] M. Salcudean, P. He, P. Nowak, I.S. Gartshore and Z. Abdullah, 1994b, *CMGFD: A Curvilinear Coordinate-based, Multigrid and Multi-Block CFD Code*, The University of British Columbia.

[49] A. Segal, P. Wesseling, J. Van Kan, C.W. Oosterlee and K. Kassels, 1992, "Invariant discretization of the incompressible Navier Stokes equations in boundary fitted coordinates", Int. J. Numer. Meth. Fluids, Vol. 15, pp. 411-426.

[50] R.K. Shah and A.L. London, *Advances in Heat Transfer*, Supplement 1, Academic Press, Inc., 1978.

[51] T. Shimizu and K. Wada, 1992, "Computer simulation and measurement of flow in a headbox", Proceedings of the Pan Pacific Pulp and Paper Technology Conference, pp. 157-165.

[52] W. Shyy, S.S. Tong and S.M. Correa, 1985, "Numerical recirculating flow calculations using a body-fitted coordinate system", Numer. Heat Transfer, Vol. 8, pp. 99-113.

[53] W. Shyy and M. Braaten, 1996, "Three-dimensional analysis of the flow in a curved hydraulic turbine draft tube", Int. J. Numer. Methods Fluids, Vol. 6, pp. 861-882.

[54] W. Shyy and C. Sun, 1993a, "Development of a pressure-correction/staggered-grid based multigrid solver for incompressible recirculating flows", Comp. Fluids, Vol. 22, pp. 51-76.

[55] W. Shyy and C. Sun, 1993b, "Multigrid computation for turbulent recirculating flows in complex geometries", Numer. Heat Transfer, B, Vol. 23, pp. 79-98.

[56] S. Sivaloganathan and G. J. Shaw, 1988, "A multigrid method for recirculating flows", Int. J. Nemer. Method in Fluids, Vol. 8, pp. 417-440.

[57] S.Syrälä, P.saarenrinne and R. Karvinen, 1988, "Fluid dynamics of a tapered manifold flow spreader", TAPPI Engineering Conference, Chicago, Illinois, pp. 223-236.

[58] K. M. Smith, W. K. Cope and S. P. Vanka, 1993, "A Multigrid procedure for three-dimensional flows on nono-orthogonal collocated grids", Int. J. Numer. Methods in Fluids, Vol. 17, pp. 887-904.

[59] J.L. Steger and R.L. Sorenson, 1979, "Automatic mesh-point clustering near a boundary in grid generation with elliptic partial differential equations". J. Comp. Phys., Vol. 33, pp. 405-410.

[60] A. M. K. P. Taylor, J. H. Whitelaw and M. Yianneskis, 1982, "Curved ducts with strong secondary motion: velocity measurements of developing laminar and turbulent flow", J. Fluids Eng., Vol. 104, pp. 350-359.

[61] J.F.Thompson, Z.U.A.Warsi and C.W.Mastin, 1982, "Boundary- fitted coordinate systems for numerical solution of partial differential equations - A Review", J. of Comp. Phys., Vol. 47, pp. 1-108.

[62] J.F.Thompson, 1984, "Grid generation techniques in computational fluid dynamics", AIAA Journal, Vol. 22, pp. 1505-1521.

[63] J.F. Thompson, Z.U.A. Warsi and C.W.Mastin, *Numerical Grid Generation, Foundations and Applications*, Elsevier, New York, 1985.

[64] P.D. Thomas and J.L. Middlecoff, 1979, "Direct control of the grid point distribution in meshes generated by elliptic equations", AIAA Journal, Vol. 18, pp. 652-656.

[65] A.D. Truffit, "Design aspects of manifold type flowspreader", 1975, Pulp and Paper Techn. Series, No. 1.

[66] S.P. Vanka, 1986a, "Block-implicit multigrid solution of Navier- Stokes equations in primitive variables", J. Compu. Phys., Vol.65, pp.138-158.

[67] S.P. Vanka, 1986b, "A calculation procedure for three-dimensional steady recirculating flows using multigrid methods", Comp. Meth. Applied Mech. Eng., Vol. 55, pp. 321-338.

[68] S. P. Vanka, 1987, "Block-implicit computation of viscous internal flows-recent results", AIAA paper No. AIAA-87-0058, New York.

[69] S.P. Vanka, 1991, "Fast numerical computation of viscous flow in a cube", Numer. Heat Transfer, Part B, Vol. 20, pp. 255-261.

[70] M. Vinokur, 1989, "An analysis of Finite-difference and Finite-Volume Formulations of conservation laws", J. Compu. Phys., Vol. 81.

[71] J. W. Yokota, 1990, "Diagonally inverted lower-upper factored implicit multigrid scheme for the three-dimensional navier-stokes equations", AIAA J., Vol. 29, pp. 1642-1649.